TYPE Original Research PUBLISHED 05 August 2025 DOI 10.3389/fcell.2025.1608400



OPEN ACCESS

EDITED BY Jidong Yan, Xi'an Jiaotong University, China

REVIEWED BY Zhihao Wu. Southern Methodist University, United States Yilin Fan. Harvard Medical School, United States

*CORRESPONDENCE

Parvana Hajieva, □ parvana.hajieva@medicalschoolhamburg.de

RECEIVED 08 April 2025 ACCEPTED 30 June 2025 PUBLISHED 05 August 2025

CITATION

Baeken MW, Borlepawar A, Kötzner P, Richly H, Behl C, Moosmann B and Hajieva P (2025) Epigenetic regulation of the respiratory chain by a mitochondrial distress-related redox signal.

Front. Cell Dev. Biol. 13:1608400. doi: 10.3389/fcell.2025.1608400

© 2025 Baeken, Borlepawar, Kötzner, Richly, Behl, Moosmann and Haijeva. This is an open-access article distributed under the terms of the Creative Commons Attribution License (CC BY). The use, distribution or reproduction in other forums is permitted, provided the original author(s) and the copyright owner(s) are credited and that the original publication in this journal is cited, in accordance with accepted academic practice. No use, distribution or reproduction is permitted which does not comply with these terms.

Epigenetic regulation of the respiratory chain by a mitochondrial distress-related redox signal

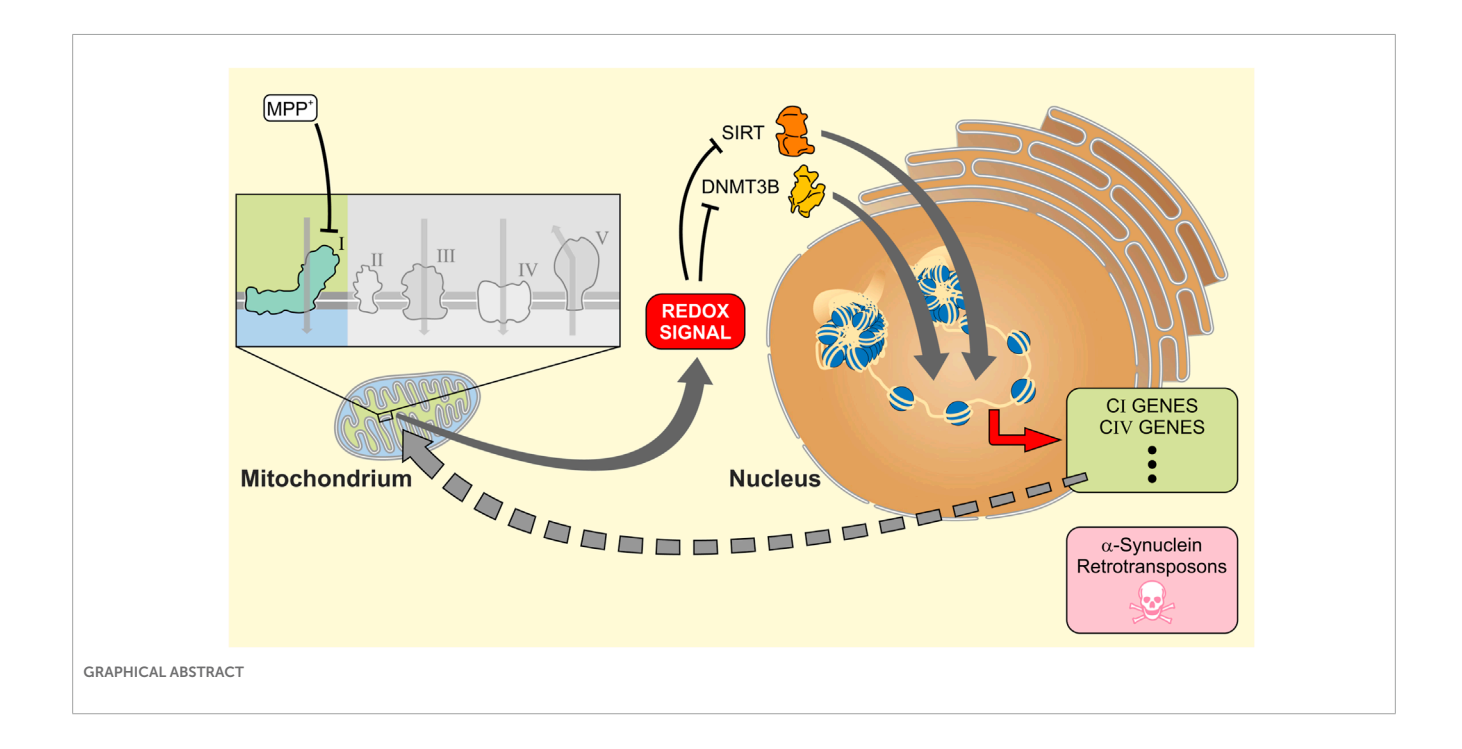
Marius W. Baeken^{1,2}, Ankush Borlepawar³, Philipp Kötzner¹, Holger Richly⁴, Christian Behl¹, Bernd Moosmann¹ and Parvana Hajieva^{1,3}*

¹Institute for Pathobiochemistry, University Medical Center of the Johannes Gutenberg University, Mainz, Germany, ²Nucleic Acid Chemistry and Engineering Unit, Okinawa Institute of Science and Technology Graduate University, Okinawa, Japan, ³Cellular Adaptation and Bioenergetics Group, Institute for Translational Medicine (ITM), MSH Medical School Hamburg, Hamburg, Germany, ⁴Laboratory of Molecular Epigenetics, Institute of Molecular Biology (IMB), Mainz, Germany

Different signaling pathways connect the mitochondrion with the transcriptional machinery in the nucleus. Redox events are thought to play a substantial role along this axis, however, many open questions about their specificity and mode of action remain. Here, we have employed subtoxic doses of the complex I inhibitor MPP+ in human neuronal LUHMES cells to characterize the contribution of scavengeable redox signals to mito-nuclear communication. MPP⁺ evoked a broadly targeted transcriptional induction of nuclear-encoded respiratory chain complex (RCC) subunits. Nanomolar doses of phenothiazine (PHT), a mitochondrially active antioxidant, attenuated these transcriptional effects by approximately half, but did not modulate the bioenergetic markers ATP, NAD+, NADH, lactate, or glucose. Transcriptional induction by MPP+ was accompanied by a loss of nuclear 5-methyl-cytosine and an increase in histone H3K14 acetylation, both of which were entirely prevented by PHT. Inhibitor and PHT reversibility experiments suggested that these alterations were mediated by lowered DNMT3B and SIRT1 levels, respectively. Analysis of MPTPtreated mice recapitulated the PHT-reversible induction of histone acetylation and DNMT3B suppression in vivo. Moreover, PHT completely abrogated the statistical significance of the association of MPP+ with the selective induction of mitochondrially imported proteins and RCC subunits. We conclude that the mitochondrion employs a redox signal to announce impending, but not yet acute mitochondrial distress to the nucleus, in order to selectively upregulate mito-metabolic genes via chromatin reorganization. Our results have implications for the interpretation of the observed epigenetic changes in Parkinson's disease and other neurodegenerative disorders.

KEYWORDS

epigenetics, MPTP, NADH dehydrogenase, Parkinson's disease, redox signaling, respiratory chain, perhydroxyl radical



Introduction

NADH dehydrogenase is the first complex of the canonic mitochondrial respiratory chain (Lenaz and Genova, 2009; Brand, 2016). Isolated complex I deficiency presents as energy generation disorder that frequently involves severe brain pathology (Kirby et al., 1999), as in the case of Leigh syndrome (Rahman et al., 1996). Less profound, structurally unexplained complex I defects appear to contribute to idiopathic Parkinson's disease (PD) (Schapira et al., 1990; Keeney et al., 2006; Gatt et al., 2016; Flones et al., 2018) and likely other neurodegenerative disorders (Swerdlow, 2020; Terada et al., 2021). Most notably, pharmacological inhibition of complex I by exogenously applied toxins can evoke a Parkinson-like syndrome in animals and man (Langston et al., 1983; Sherer et al., 2007; Cannon and Greenamyre, 2011; Langston, 2017; Zeng et al., 2018) that in some models authentically recapitulates idiopathic PD (Betarbet et al., 2000; Cannon et al., 2009). Genetic mouse models of PD have not attained a comparable degree of authenticity yet (Dawson et al., 2010; Creed and Goldberg, 2018; Chia et al., 2020). Among the complex I inhibitor-based models of PD, the MPTP/MPP⁺ model is the oldest (Langston et al., 1983; Langston, 2017) and arguably most widely employed model (Moosmann and Behl, 2002; Gibrat et al., 2009). Its dopaminergic cytotoxicity is essentially attributed to oxidative stress caused by the complex I inhibition (Johannessen et al., 1986; Ramsay et al., 1987; Sayre et al., 2008; Hajieva et al., 2009).

Apparently unrelated to these lines of research, various epigenetic changes have been described to occur in PD. Specifically, decreased levels of global DNA cytosine methylation have been observed in *post mortem* brains from patients with PD and the related entity, dementia with Lewy bodies (Desplats et al., 2011). The effect was confirmed in CpG islands of regulatory regions of several disease-relevant genes, including the promotor and the first intron of α -synuclein (Jowaed et al., 2010; Matsumoto et al.,

2010; Desplats et al., 2011), and in a number of other, potentially disease-related genes such as CYP2E1 (Kaut et al., 2022; Schaffner and Kobor, 2022). Characteristically altered, mostly decreased DNA methylation may also occur in blood cells from PD patients, suggesting a systemic phenomenon (Masliah et al., 2013).

Increased histone lysine acetylation is another notable epigenetic alteration in idiopathic PD. For instance, significant increases in H3K14 and H3K18 acetylation have been observed in the motor cortex of PD patients (Gebremedhin and Rademacher, 2016). These increases were yet contrasted by a decrease in H3K9 acetylation (Gebremedhin and Rademacher, 2016), which has been confirmed for the substantia nigra in unrelated PD cases (Harrison et al., 2018). Several other lysines have been found to be hyperacetylated in midbrain tissue (Park et al., 2016) and in the cerebral cortex (Toker et al., 2021) of idiopathic PD patients, the most prominent of which were H3K27 and, again, H3K14 (Toker et al., 2021). In summary, various histone lysines seem to be prone to hyperacetylation in PD. However, there is no consensus whether increased histone acetylation and the thereby induced transcriptional facilitation is adverse-pathologic (Park et al., 2016; Toker et al., 2021) or rather adaptive-protective (Kidd and Schneider, 2010) in the disease.

A connection between the two aforementioned signature elements of PD, complex I inhibition and epigenetic (dys)regulation, has been suggested by a small number of pioneering studies that have evidenced altered DNA methylation and histone acetylation in the wake of pharmacological complex I inhibition (Feng et al., 2015; Park et al., 2016; Yang et al., 2017). However, the purposefulness and origin of the potentially adverse (Matsumoto et al., 2010; Baeken et al., 2020; Toker et al., 2021) epigenetic transcriptional facilitation in PD has remained elusive. Hence, we have analyzed in detail the transcriptomic events in human neuronal dopaminergic LUHMES cells after complex I inhibition. We find that mitochondria challenged in this way release a redox signal that is responsible

for the selective transcriptional upregulation of mitochondrially imported gene products, particularly respiratory chain complex (RCC) subunits. We further characterize the mechanism of this adaptive upregulation as primarily epigenetic and related to DNMT3B and SIRT1 inhibition.

Results

Complex I inhibition evokes a widespread induction of nuclear-encoded RCC subunits in the absence of ATP depletion

The compound MPP+ (1-methyl-4-phenylpyridinium) is a frequently used reference tool for eliciting experimental complex I deficiency (Beal, 2001; Richardson et al., 2005; Langston, 2017). To ensure selectivity and avoid toxicity of this drug, differentiated human LUHMES cells were treated with $10\,\mu\text{M}$ MPP+ for $48\,\text{h}$, following closely related protocols (Krug et al., 2014; Smirnova et al., 2016). No overt signs of cytotoxicity were induced by this treatment regimen as reported (Krug et al., 2014; Baeken, 2020; Baeken et al., 2021); however, a moderate degree of microtubular reorganization was visible using immunocytochemistry (Supplementary Figure S1). Transcriptomic analysis of the MPP+-treated cultures indicated that the majority of RCC subunits were transcriptionally induced by complex I inhibition, consistent with a functional, compensatory response (Figure 1A; Supplementary Table S1) affecting many distant genomic loci (Supplementary Figure S2). Specifically, 28 out of 37 complex I genes were significantly upregulated (Figure 1D), as were 9 out of 10 complex III genes (Figure 1F), 11 out of 11 complex IV genes (Figure 1G), and 14 out of 16 complex V genes (Figure 1H). On average, global transcription of complex I genes was induced by 61%, complex III genes by 106%, complex IV genes by 123%, and complex V genes by 76%.

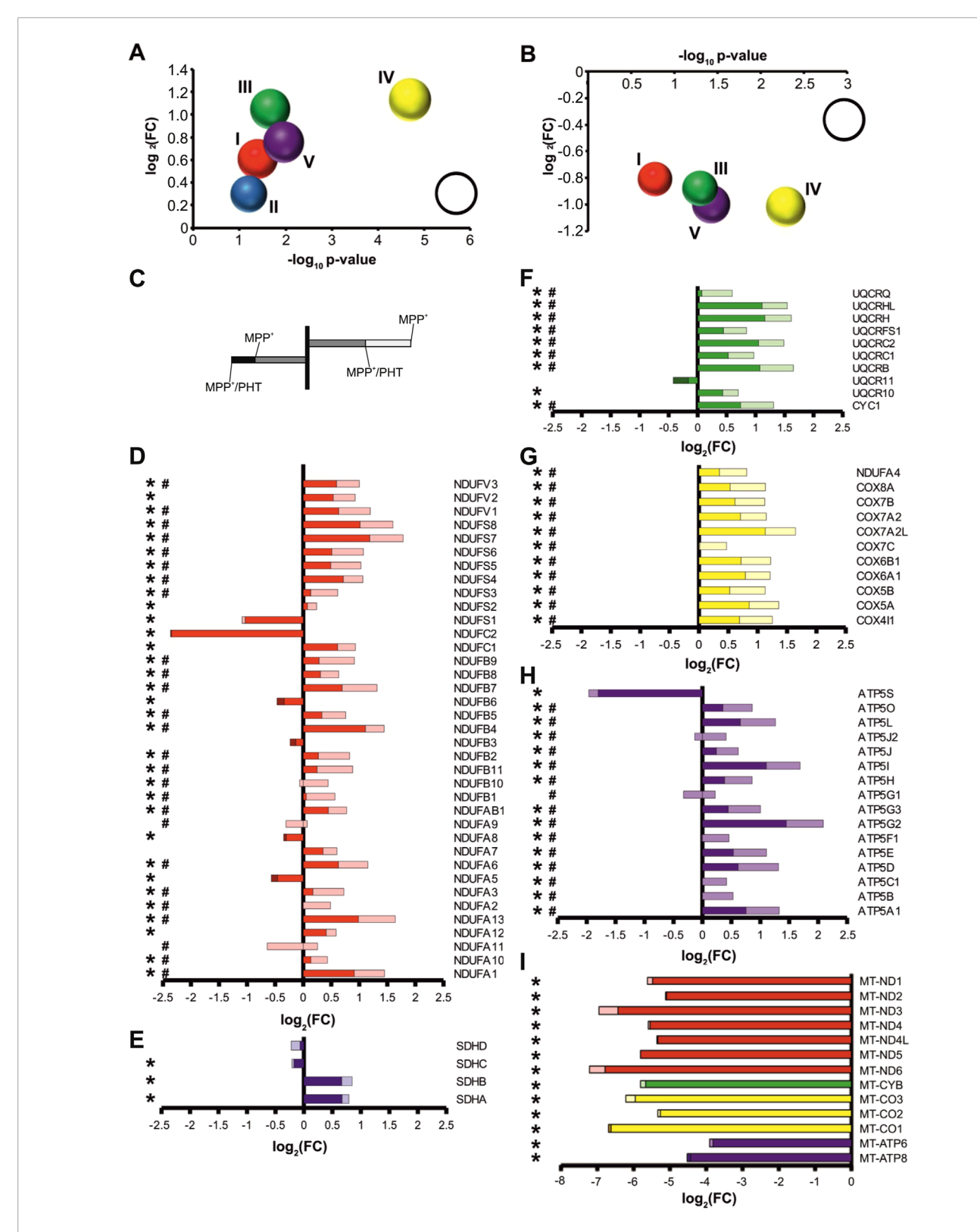
In inhibiting complex I electron flow from the aqueous NADH oxidation site to the ubiquinone binding site, MPP+ evokes two major biochemical effects: the loss of complex I as a proton pump contributing to ATP generation, and the production of superoxide radicals and other reactive oxygen species (ROS) (Fallon et al., 1997; Beal, 2001; Richardson et al., 2005). To distinguish which of these effects caused the transcriptional changes, we applied the mitochondrial antioxidant phenothiazine (PHT) to MPP+treated cells. PHT is a nanomolar-activity antioxidant compound that permeates mitochondria and has shown high efficacy against mitochondrial ROS even in models where classic phenolic antioxidants generally fail (Hajieva et al., 2009; Mocko et al., 2010; Tapias et al., 2019). Concomitantly, PHT is not a twoelectron reductant, meaning that it does not shuttle electrons from inhibited complex I to complex IV such as methylene blue (Atamna et al., 2008; Ohlow and Moosmann, 2011). Thus, it cannot ameliorate bioenergetic deficits, but merely acts as an ROS scavenger.

PHT treatment caused a significant, apparently uniform attenuation of the transcriptional effects of MPP⁺ (Figure 1B; Supplementary Table S1). More specifically, 26 out of 37 complex I genes were significantly downregulated compared to MPP⁺ only-treated cells (Figure 1D), as were 8 out of 10 complex III genes (Figure 1F), 11 out of 11 complex IV genes (Figure 1G), and 15 out of

16 complex V genes (Figure 1H). Across all subunits, transcription of complex I genes was reduced by 40%, complex III genes by 44%, complex IV genes by 51%, and complex V genes by 50%. Hence, approximately half of the regulatory effect of complex I inhibition was prevented by a low nanomolar dose of PHT. This may be considered a rather high fraction since kinetic scavenging systems can never intercept with all radicals if the radicals' targets are present at the biologically typical, μM to μM concentrations (Moosmann and Hajieva, 2022).

Notably, mitochondrially encoded transcripts were severely reduced following MPP+ treatment (Figure 1I), consistent with earlier reports (Krug et al., 2014). Potentially, the engagement of the cells in preparatory mitochondrial DNA replication, which is known to be incompatible with mitochondrial transcription (Agaronyan et al., 2015), accounts for this effect. The mitochondrial transcripts were also unresponsive to PHT treatment like most of the nuclear encoded transcripts, indicating their disparate, redox-independent regulation. Interestingly, the three most prominently suppressed nuclear encoded RCC-related genes were either supernumerary, regulatory subunits involved in RCC assembly, like ATP5S (Belogrudov, 2009) and NDUFC2 (Alahmad et al., 2020), or they regulate supercomplex formation and have additional functions in the cytosol, like NDUFS1 (Elkholi et al., 2019). Evidently, assembly factors are less required as long as mitochondrial transcription and translation do not proceed.

To experimentally ascertain the supposed non-interference of PHT with cellular bioenergetics under the employed conditions, LUHMES cells treated identically as before were surveyed for a series of functional metabolic readouts. As shown in Figure 2, MPP+ treatment had no significant effect on cellular ATP levels, with or without PHT coadministration (Figure 2A). NAD+ levels were also unchanged (Figure 2B), while NADH levels were increased by complex I inhibition as expected (Figure 2C), resulting in a significant drop in the NAD+/NADH ratio relevant for metabolic flux (Figure 2D). PHT had no modulatory effect on any of these parameters. Likewise, PHT did not alter the anticipated effects of MPP+ on lactate production (Figure 2E) and the acidification of the medium (Figure 2F), and it had an only minor modulatory effect on 2 out of 5 of the detected carbonic anhydrases (Supplementary Figure S3A). Hence, PHT did not prevent the expectable induction of anaerobic glycolysis by MPP+, which was further evidenced by an accelerated disappearance of glucose in the medium (Figure 2G) and an induction of the neuron-specific glucose transporter GLUT3 (Figures 2H,I). After all, the drop in membrane potential typical for complex I inhibition by MPP+ (Hajieva et al., 2009; Krug et al., 2014) was also only partially attenuated by PHT (Figures 2J,K). In contrast, analysis of cellular ROS levels by means of two indicator dyes, the untargeted sensor CellROX, and the mitochondrion-specific sensor MitoROX, clearly demonstrated the prooxidant effect of MPP+ and the antioxidant effect of PHT (Figures 2J,L,M), as widely reported (Beal, 2001; Hajieva et al., 2009; Mocko et al., 2010; Tapias et al., 2019). In summary, PHT was incapable of substantially modulating the bioenergetic effects of complex I inhibition, but selectively blunted the ensuing ROS effect. Besides, it had a small enhancing effect on the NAD+/NADH ratio at baseline (Figure 2D).



Redox-dependent transcriptional induction of nuclear-encoded RCC subunits following complex I inhibition. Transcriptional changes were measured by RNA sequencing of differentiated LUHMES cells treated with 10 μ M MPP+ (a complex I inhibitor) and 20 nM PHT (a mitochondrial antioxidant) for 48 h. (A) Bubble diagram summarizing the regulation of RCC subunits after MPP+ treatment. Each bubble represents all nuclear subunits of one RCC (I-V). The bubble position on the y-axis indicates the \log_2 mean of the transcriptional fold changes (FC), the bubble position on the x-axis indicates the $-\log_{10}$ mean of the associated p values (n = 3, one-way ANOVA). The bubble size indicates the percentage of significantly regulated transcripts (reference bubble = 100%). (B) Corresponding bubble diagram summarizing the effect of PHT on MPP+-treated cells. (C) Instructional sketch for the color-coded bar graphs in D-I. Regulation after MPP+ is indicated by total bar length or, where applicable, bar length to a darker color. Regulation after (Continued)

FIGURE 1 (Continued)

PHT/MPP⁺is indicated by color coding: lighter color denotes that the MPP⁺effect was reduced by PHT, darker color denotes that the MPP⁺effect was increased by PHT. (**D**) Individual regulation of nuclear-encoded complex I subunits. Symbols indicate: *p-value ≤0.05 for MPP⁺vs. control, #p-value ≤0.05 for PHT/MPP⁺vs. MPP⁺by one-way ANOVA (n = 3) in all panels of this figure. (**E**) Individual regulation of complex II subunits. (**F**) Individual regulation of nuclear-encoded complex II subunits. (**G**) Individual regulation of nuclear-encoded complex V subunits. (**I**) Regulation of mitochondrially encoded RCC subunits.

MPP⁺ causes global DNA hypomethylation through DNMT3B insufficiency that is responsive to the antioxidant PHT *in vitro*

Considering the rather uniform patterns of up- and downregulation of numerous functionally related genes (Figure 1) scattered all over the genome (Supplementary Figure S2), we hypothesized that epigenetic mechanisms might be involved. Indeed, reduced levels of DNA methylation have been reported in different models of PD and in patient-derived tissue (Desplats et al., 2011; Yang et al., 2017), and several key enzymes of the epigenetic machinery are known to be modulated by ROS (Chen and Shen, 2025). Consistently, MPP⁺ caused a substantial reduction of global 5-methylcytosine levels in the nucleus of differentiated LUHMES cells within 48 h (Figures 3A,B). This effect was abrogated by PHT cotreatment. The control drug 6-thioguanine, an established DNA methylation suppressor (Agrawal et al., 2018), elicited comparable effects at the employed standard concentration of 1 µM (Mender et al., 2015).

DNA methylation in humans is established by three DNA methyltransferases. DNMT1 is considered a maintenance protein requiring a hemi-methylated template, whereas DNMT3A and DNMT3B are de novo methyltransferases (Hermann et al., 2004). Immunocytochemical analysis indicated that these proteins were variably localized to the nucleus in differentiated LUHMES cells (between 30% and 60%) (Figures 3A,B). Notably yet, all three proteins exhibited a significant shift away from the nucleus upon MPP+ exposure (Figures 3A,B), as also reported for DNMT1 in PD (Desplats et al., 2011). These effects were not rescued by PHT cotreatment except in the case of DNMT3B, which was therefore putatively assigned to be responsible for the observed, reversible changes in DNA methylation. The compound 6thioguanine had a similar effect on the localization of DNMT1 and DNMT3A as MPP+, but did not influence DNMT3B. The former observation is consistent with the reported induction of proteasomal degradation of DNMT1 by 6-thioguanine (Yuan et al., 2011), which may also affect DNMT3A (Huang et al., 2022), but potentially spares DNMT3B. The reduction of nuclear DNMT expression by MPP+ may have been exacerbated by the pronounced transcriptional downregulation of genes controlling the production of the methylation cofactor, S-adenosyl methionine (Supplementary Figures S3B, C). These transcriptional effects were also relatively PHT-sensitive.

DNMT3B expression in the Western blot showed two bands at ~95 kDa (DNMT3BL) and ~72 kDa (DNMT3BS) (Figures 3C,D). MPP+ caused a modest decline of both isoforms by approximately 30%, which was prevented by PHT treatment, but significantly only for DNMT3BS, the major form of DNMT3B in these cells. Exclusive PHT treatment also significantly increased DNMT3BS expression compared to the control group (Figures 3C,D) without

rescuing DNMT3B at the mRNA level (Figure 3E). These data suggest that mitochondrial ROS lead to a loss of DNMT3B in the nucleus through a loss of protein expression, amplified by a shift of the remaining protein out of the nucleus. Like other epigenetic effector proteins (Park et al., 2016; Baeken et al., 2021; Baeken, 2024), DNMTs are now well established to be regulated by their controlled proteolytic degradation (Du et al., 2010; Yuan et al., 2011; Huang et al., 2022), which may also account for the current observations. Moreover, DNMT3A/3B have been shown in the past to be functionally affected by the thiol redox state of the cell (Chen et al., 2012). The PHT-indifferent baseline suppression of DNMT1 and DNMT3B transcription by MPP+ (Figure 3E) probably relates to another biochemical mechanism.

MPP⁺ causes global lysine hyperacetylation through SIRT1 suppression that is responsive to the antioxidant PHT *in vitro*

Histone lysine acetylation appears to be widely induced in idiopathic PD (Gebremedhin and Rademacher, 2016; Park et al., 2016; Toker et al., 2021) and in models of PD based on complex I inhibition (Park et al., 2016). Of the many sites that appear to be hyperacetylated in PD, including H2K15, H3K14, H3K18, H3K27 and H4K5, the site H3K14 may represent one of the most reproducible disease markers. No conflicting data as for H3K9 have been reported for H3K14 (Gebremedhin and Rademacher, 2016; Park et al., 2016), and it may also be more robustly induced than the related, more widely explored H3K9 site (Karmodiya et al., 2012). H3K14 has not been investigated after complex I inhibition.

Treatment of LUHMES cells with MPP+ as before evoked a significant increase in total lysine acetylation as well as H3K14 acetylation, which were entirely prevented by PHT cotreatment and thus redox-related (Figures 4A-D). The increase in H3K14 acetylation as per Western blot (~600%) (Figure 4C) vastly exceeded the increase in total lysine acetylation (~30%) (Figure 4D). Two minimally modified PHT derivatives that essentially lack antioxidant activity (Hajieva et al., 2009), namely, Nmethylphenothiazine (MPHT) and N-acetylphenothiazine (APHT), were also tested in this assay because putatively involved histone deacetylases of the sirtuin (SIRT) family are highly sensitive to the levels of the somewhat related heteroaromatic molecule NAD+, containing nicotinamide (Anderson et al., 2017). MPHT and APHT were clearly less potent than PHT in their prevention of lysine acetylation (Figures 4C,D), corroborating that the PHT effect was caused by antioxidation.

To further define the cause of MPP⁺-induced hyperacetylation, we employed trichostatin A (TSA), an inhibitor of Zn²⁺-dependent histone deacetylases (HDACs), and selisistat (EX-527), a SIRT1 inhibitor with approximately 200-fold selectivity against SIRT2

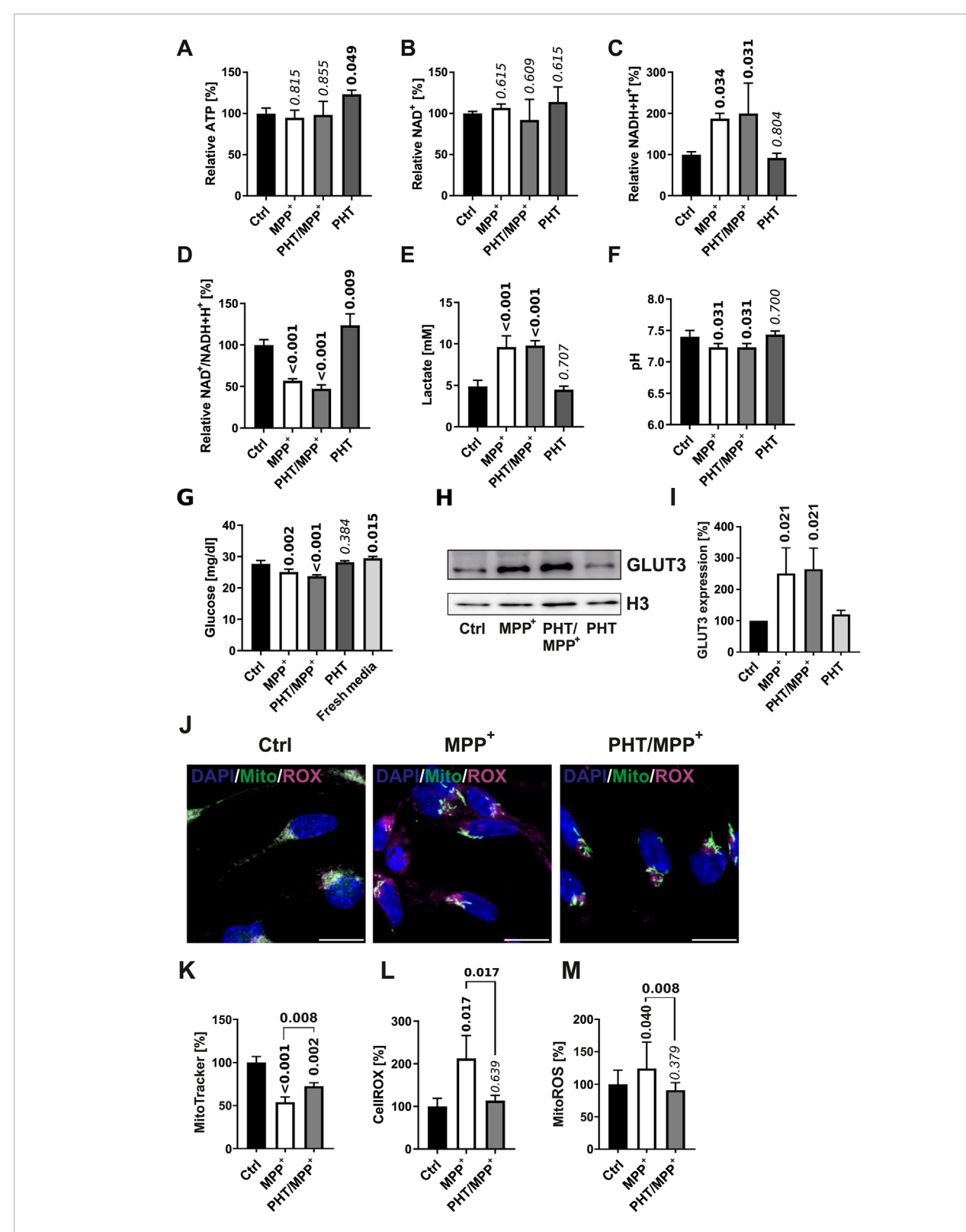


FIGURE 2
Bioenergetic and redox changes evoked by complex I inhibition. (A) Relative ATP levels in cells treated with 10 μ M MPP⁺ and 20 nM PHT for 48 h as in the experiment in Figure 1. Numbers atop of the bars indicate the level of significance versus the control as determined by two-way ANOVA and Benjamini-Hochberg post hoc test. Bold numericals highlight p \leq 0.05. All standard deviations in this figure result from n = 3 experiments. (B) Relative levels of NAD⁺ in cells treated as before. (C) Relative levels of NADH+H⁺ in the same cells. (D) The NAD⁺/NADH+H⁺ ratio in the same cells. (E) Lactate concentrations in 48 h culture media from corresponding cells. (F) Level of acidification in 48 h culture media from cells treated as before. (G) Glucose concentrations in 48 h culture media from cells treated as before. Fresh media were assayed for control purposes. (H) Western blotting of the glucose transporter GLUT3 and histone H3 in cells treated with 10 μ M MPP⁺ and 20 nM PHT as before. (I) Densitometric quantification of n = 3 GLUT3 blots

FIGURE 2 (Continued)

normalized on H3. (J) Fluorescence images (x63 magnification) of LUHMES cells treated as before, administered with the ROS indicator compound CellROX (magenta), MitoTracker Red (green), and the chromatin stain DAPI (blue). The scale bars denote $10 \,\mu\text{m}$. (K) Densitometric image quantification of MitoTracker fluorescence intensity normalized to the number of cells assayed (n = 3, number of cells per n: 50-100, one-way ANOVA). (L) Densitometric image quantification of CellROX fluorescence normalized correspondingly (n = 3, number of cells per n: ~50, one-way ANOVA). (M) MitoROX fluorescence in living cells treated as before. Fluorescence intensity was quantified with a plate reader 30 min after loading of the dye (n = 14, one-way ANOVA).

and SIRT3 (Yoshida et al., 1990; Napper et al., 2005). Analysis of global lysine acetylation by immunocytochemistry (Figure 4B) and image quantification (Figure 4E) indicated that both agents caused an increase in lysine acetylation by approximately 50% and, thus, resembled MPP⁺ quantitatively. However, these increases were resistant to antioxidant PHT treatment as expected. Additive treatment with the inhibitors plus MPP⁺ gave a further (and PHT-reversible) increase only with TSA, but not with EX-527 (Figure 4E). Thus, the effect of MPP⁺ was concluded to be mediated by EX-527-inhibited deacetylases, but not by TSA-inhibited deacetylases.

Investigation of SIRT1 by Western blot (Figures 4F,G) indicated that this protein was significantly reduced upon MPP+-treatment in a PHT-reversible fashion; a corresponding result was obtained with a direct, fluorescent SIRT1 activity assay using cell lysates (Figure 4H). Here, the enzyme activity loss in the lysate was partially prevented by PHT, but unaltered by MPHT. In view of the unchanged transcription of SIRT1 (Figure 4I), these results demonstrate a reduction of the SIRT1 protein and of its enzyme activity due to a redox signal induced by mitochondrial complex I inhibition. The loss of this protein may be attributable to the redox-dependent induction of autophagic degradation of most sirtuins by MPP+ as recently reported (Baeken et al., 2021). Because SIRT1 enzyme activity is also known to be negatively affected by direct cysteine oxidation (Shao et al., 2014; Kalous et al., 2020), it is possible that both mechanisms operate in parallel.

MPTP causes ROS-dependent epigenetic changes *in vivo*

Redox biological experiments in cell culture involve the general danger of returning exaggerated effects due to an unphysiologically oxidative environment (Kunath et al., 2020). Hence, we have tested the validity of some of the described molecular events in a mouse model of PD based on the same initiating event, namely, complex I inhibition by MPP⁺. Therefore, the pro-toxin MPTP (Beal, 2001; Langston, 2017) was administered intraperitoneally to 10-week-old male C57Bl/6J mice as sketched in the scheme in Figure 5. PHT was administered orally, including a roll-in period (for details, compare the Materials and Methods). Doses were chosen as to obtain an intermediate degree of toxicity only in the particularly vulnerable region, substantia nigra (SN), because widespread cell death could arguably give rise to strong secondary effects.

To verify the efficacy and selectivity of the employed MPTP dose and to probe any potential prevention by PHT, we analyzed the expression of tyrosine hydroxylase (TH), a commonly adopted marker of dopaminergic cell viability *in vivo* (Beal, 2001; Langston, 2017). Hence, midbrain slices were immunostained with antibodies against TH and counterstained with the chromatin dye Hoechst

33,258. The staining revealed a visible drop in the number of TH-positive cells in the SN, the primary region affected in PD (Figure 5A). The adjacent and larger ventral tegmental area (VTA) was essentially spared from toxicity as expected (Beal, 2001). Quantification by image analysis involving cell-cell border demarcation and counting of TH-positive cells yielded approximately 50% loss of SN neurons, with PHT treatment affording almost complete protection (Figure 5B), as already reported in related models (Mocko et al., 2010; Tapias et al., 2019). Motor performance experiments ("Rotarod") done with the animals before sacrifice suggested a variable decline of capabilities from MPTP treatment including rescue by PHT, but statistical significance was not reached (Figure 5C).

Analysis of H3K14 acetylation in the SN demonstrated that MPTP treatment triggered this modification in vivo in a PHT-reversible fashion, with an increase of about 50% as per immunocytochemistry (Figures 6A,C) and about 150% as per Western blot (Figures 6B,D). Global lysine acetylation as per Western blot was raised by about 50% (Figure 6E). These results recapitulate the human cell culture outcome (Figure 4), but in an attenuated fashion. However, SIRT1 expression in the mouse in vivo was not decreased, but rather increased (Figure 6F). As PHT did not revert this effect, a redox-unrelated mechanism may have dominated here. Two additional SIRTs known to be rapidly degraded in vitro after MPP+ treatment (Baeken et al., 2021) were probed for control purposes, and indeed, SIRT3 and SIRT4 were suppressed by about 30% and 20%, respectively, and PHT-reversibly in vivo (Figures 6G,H). The origin of the differential behavior of SIRT1 is unclear at present. DNMT3B expression, in turn, was decreased in vivo by about 30% and rescued by PHT administration (Figure 6I), which recapitulates the in vitro situation. In summary, these results confirm the operability of a redox signal targeting epigenetic regulator proteins after complex I inhibition in vivo.

The transcriptomic effects of the MPP⁺-induced redox signal are specific for mitochondrial targets and purposefully related genes

From the results presented so far, the hypothesis was derived that the redox-dependent effect of complex I inhibition towards the epigenetic effectors SIRT and DNMT3B may be part of a regulatory cycle to specifically maintain mitochondrial metabolic functioning. This hypothesis was tested by revisiting the transcriptomic changes that accompanied the induction of most RCC subunits as described in Figure 1. Out of 15,168 genes recovered in the RNA sequencing experiment, 3639 were upregulated, and 3531 were downregulated. A total of 826 genes coding for mitochondrially

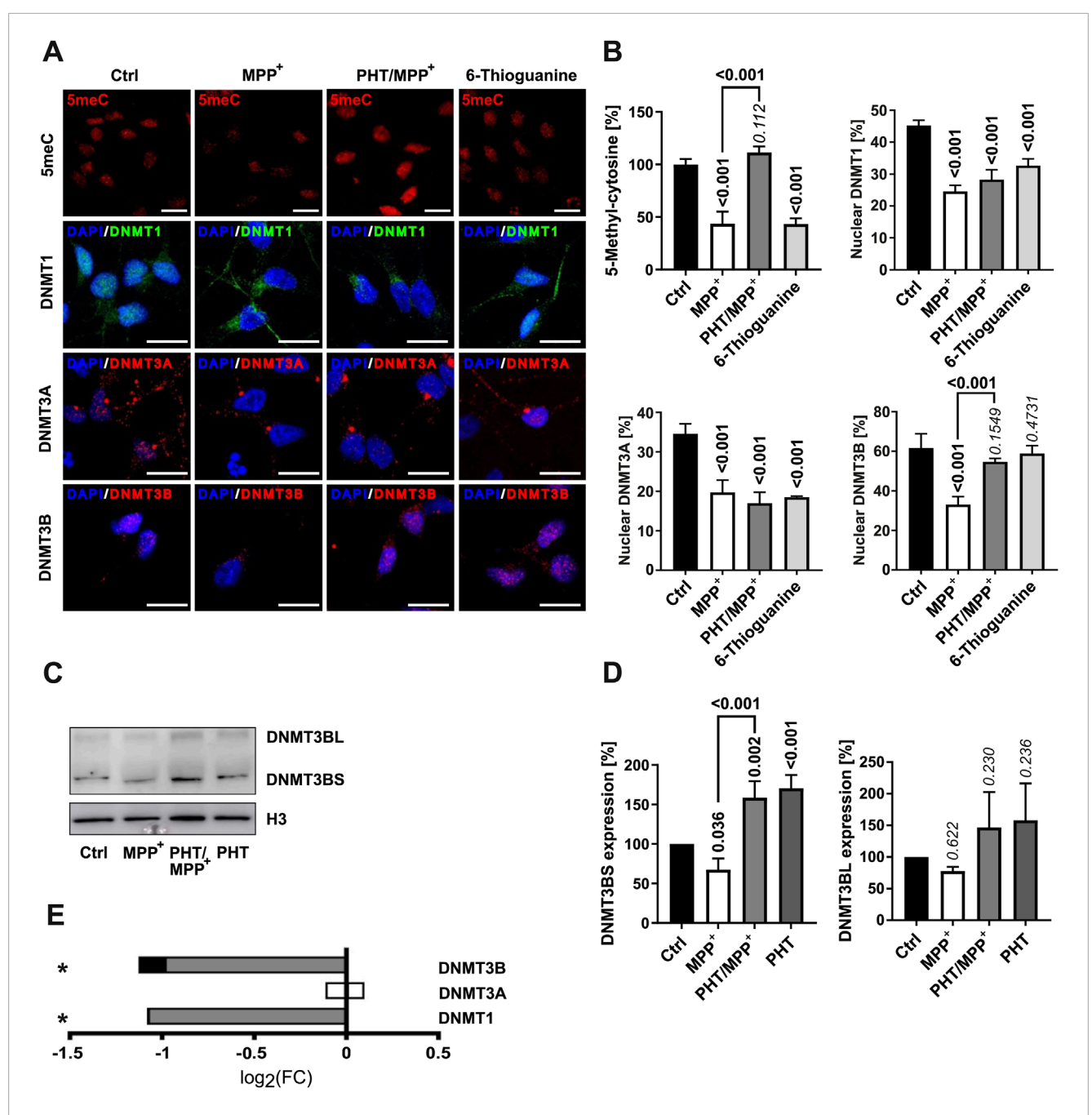


FIGURE 3 Changes in DNA methylation and DNMT localization. (A) Fluorescence microscopic images of immunostained LUHMES cells treated with 10 μ M MPP⁺, 20 nM PHT, or 1 μ M 6-thioguanine over 48 h (×63 magnification). In the first row, 5-methylcytosine (5meC) is visualized in red. The other rows depict the DNA methyltransferases DNMT1 (green), DNMT3A (red), and DNMT3B (red) as indicated. The blue staining represents the chromatin dye DAPI. The scale bars denote 20 μ m. (B) Bar graph diagrams of densitometric quantifications of images (n = 3, number of cells per n: 50–100) as shown in A. DNMT subcellular localization (nuclear vs. cytosolic) was determined from the fraction of the signal intensity that colocalized with DAPI. P values atop of the bars and bold numericals (p \leq 0.05) are used as in Figure 2. (C) Western blotting of DNMT3B and histone H3 in cells treated with 10 μ M MPP⁺ and 20 nM PHT as before. DNMT3B featured two bands at ~100 kDa (DNMT3BL) and ~70 kDa (DNMT3BS). (D) Densitometric quantification of n = 3 DNMT3B blots normalized on H3. (E) Transcriptional regulation of the DNMTs. Symbols indicate: *p-value \leq 0.05 for MPP⁺ vs. control. Shading of the fill color is used to denote PHT effects as in Figure 1.

imported proteins ("MitoGenes") as well as 78 RCC complex genes were selected for statistical analysis.

Mitogenes were found to be significantly more highly expressed after MPP⁺ treatment than average genes. Of these mitogenes, RCC complex genes were significantly more highly expressed than the

other genes (Figure 7A). Hence, complex I inhibition caused a selective increase in the transcription of genes counteracting any potential malfunction of complex I and the respiratory chain. The selective targeting of mitogenes and RCC complex genes by MPP+ was also selectively affected by PHT treatment: coadministration

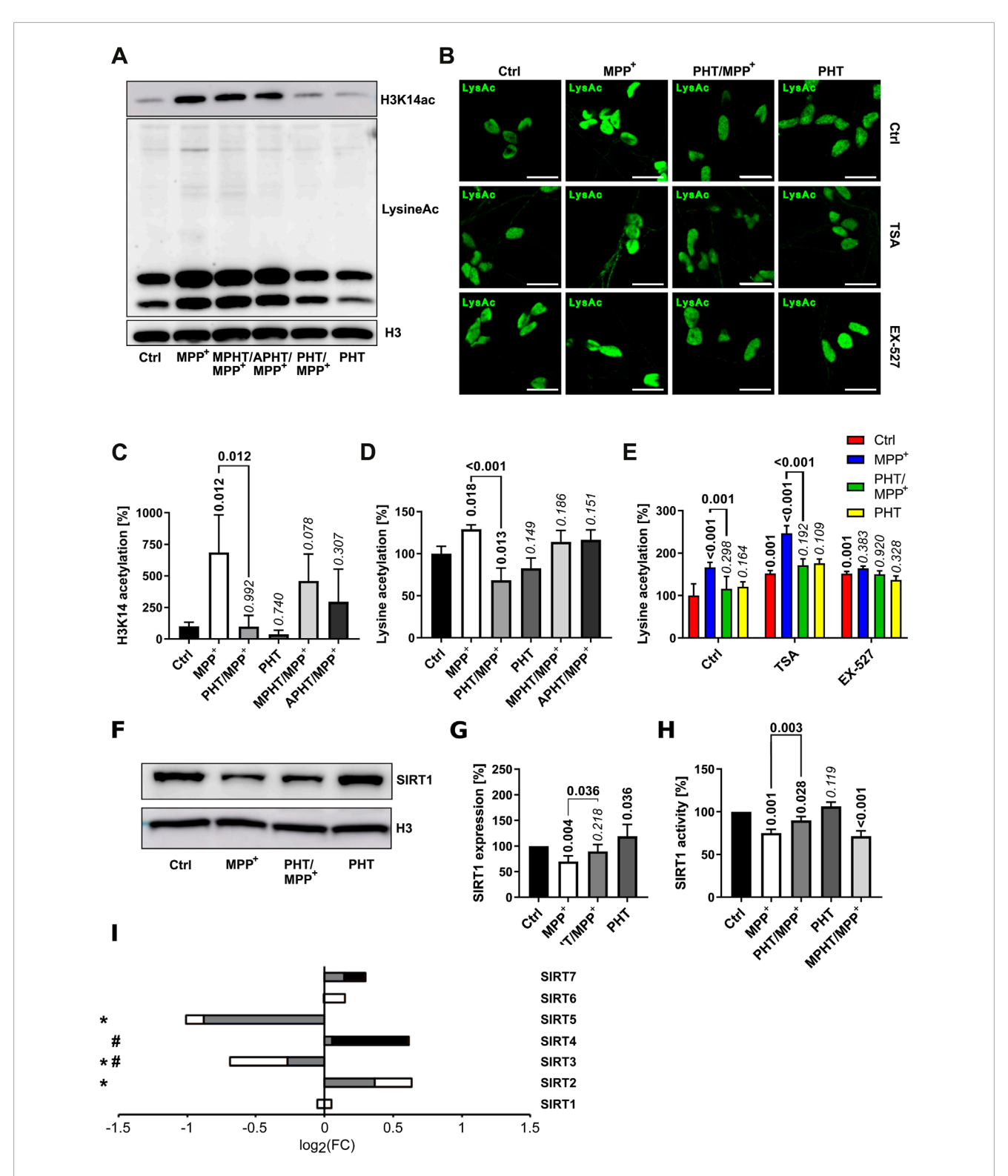
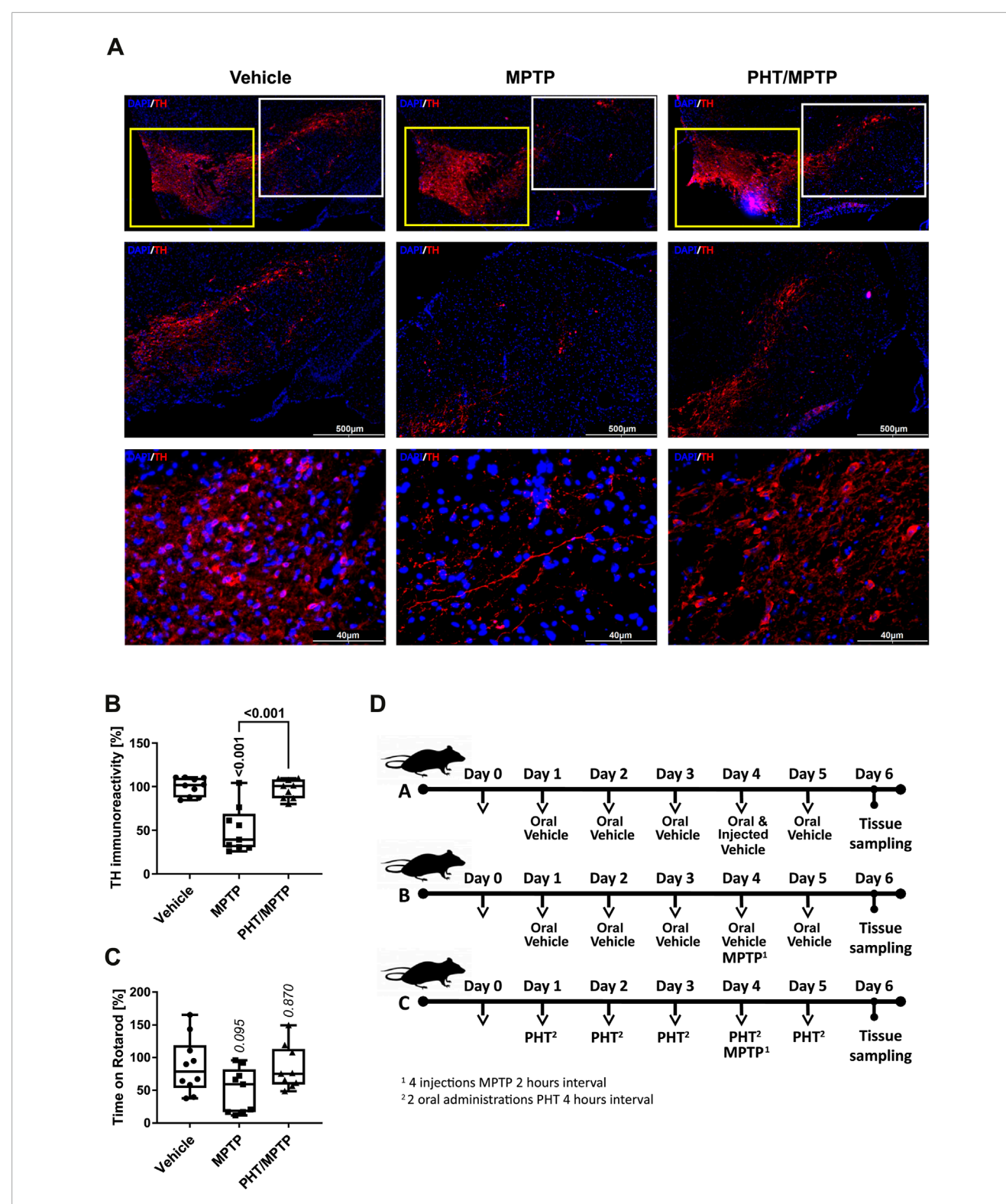


FIGURE 4
Lysine acetylation and deacetylase expression. Lysine acetylation and the expression of selected deacetylases was investigated in LUHMES cells treated with 10 μ M MPP+ and 20 nM PHT for 48 h as before. MPHT and APHT are two inactive PHT congeners used at 20 nM concentration as PHT. (A)
Western blotting against H3K14ac, total acetylated lysine and H3. (B) Microscopic images (x63 magnification) of cells immunostained for total lysine acetylation. TSA (50 nM) and Ex-527 (100 nM) are (class-)specific deacetylase inhibitors. The scale bars denote 20 μ m. (C) Densitometric quantification of Western blotts (n = 3) against H3K14ac as shown in A, normalized on H3. (D) The same quantification (n = 3) done for total lysine acetylation. (E)
Quantification of lysine acetylation by image analysis of immunostained cells as shown in B (n = 3, number of cells per n: 50–100). (F) Western blotting of the NAD-dependent deacetylase SIRT1 and H3. (G) Densitometric quantification of n = 3 SIRT1 blots normalized on H3. (H) SIRT1 deacetylase activity determined in lysates of differentiated LUHMES cells (n = 3). (I) Transcriptional regulation of all sirtuins detected in LUHMES cells by RNA sequencing. Symbols indicate: *p-value \leq 0.05 for MPP+ vs. control, #p-value \leq 0.05 for PHT/MPP+ vs. MPP+. Shading of the fill color is used to denote PHT effects as in Figure 1.



General characterization of the MPP $^+$ /PHT system *in vivo*. Male, wild-type, 10-week old C57Bl/6J mice were treated with the metabolic MPP $^+$ -precursor MPTP and analyzed behaviorally and biochemically. (A) Fluorescence immunohistochemistry of midbrain slices stained for the dopaminergic marker tyrosine hydroxylase (TH, red), counterstained with Hoechst 33,258 ('DAPI', blue). The upper row shows an overview of the rostral midbrain depicting the ventral tegmental area (VTA; yellow boxes) on the left, and the substantia nigra (SN; white boxes) on the right. The middle row depicts low-magnification images of the overall SN, the lower row shows high-magnification images from the central part of the SN. (B) Quantification of TH immunoreactivity in sections from all treatment groups (n = 9 $^-$ 10 animals, with each symbol representing one animal). (C) Rotarod performance of the different animals (n = 9 $^-$ 10 animals). Rotarod is a widely employed motor diagnostic test in the study of Parkinsonism. (D) Schematic overview of the different treatment groups. Group A received two types of vehicles (oral vehicle and injected vehicle), group B received oral vehicle and MPTP, and group C received PHT and MPTP (including a PHT roll-in period) as displayed. Note that PHT was administered orally (in 2% DMSO in corn oil), whereas MPTP was injected intraperitoneally (in 0.9% saline).

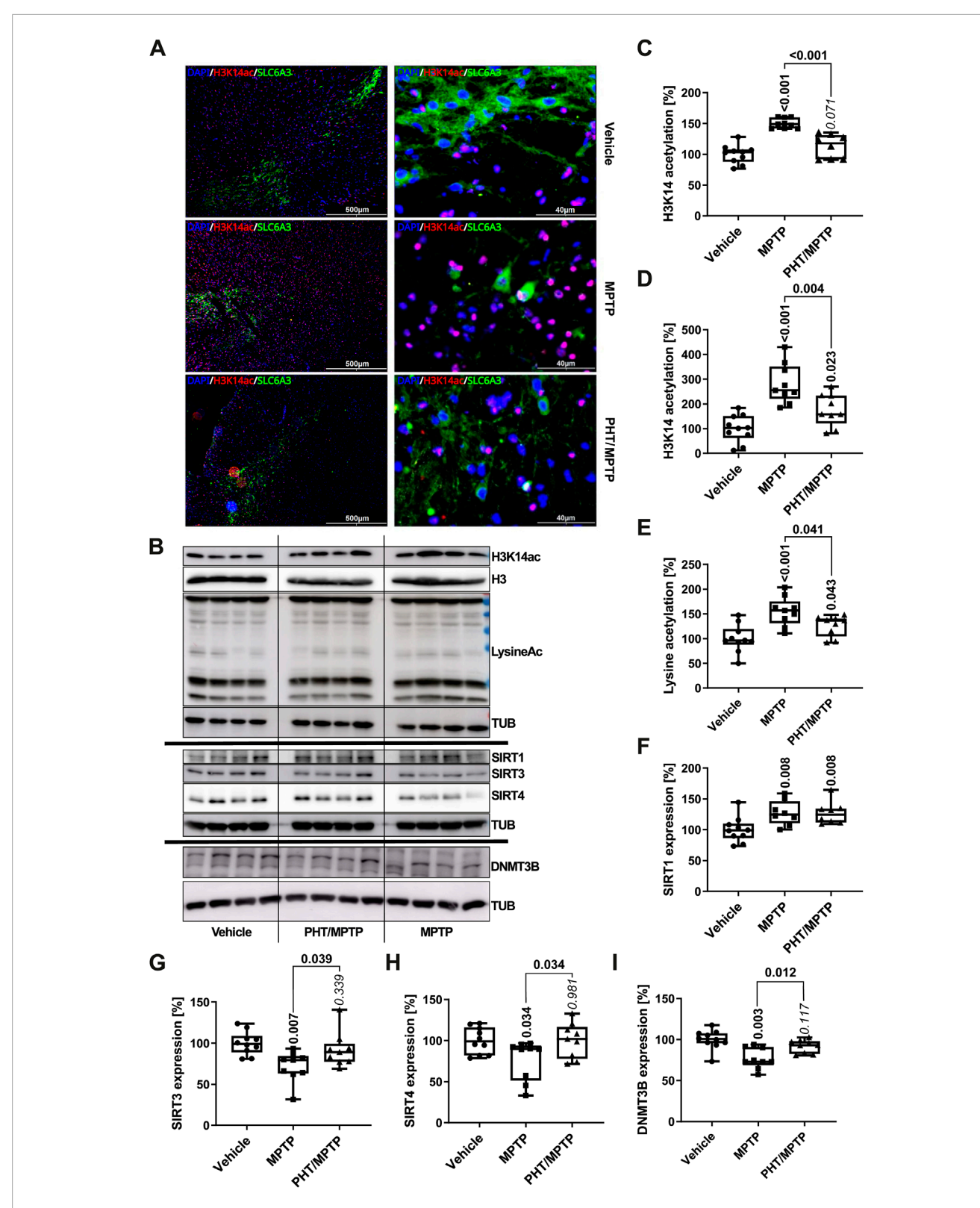
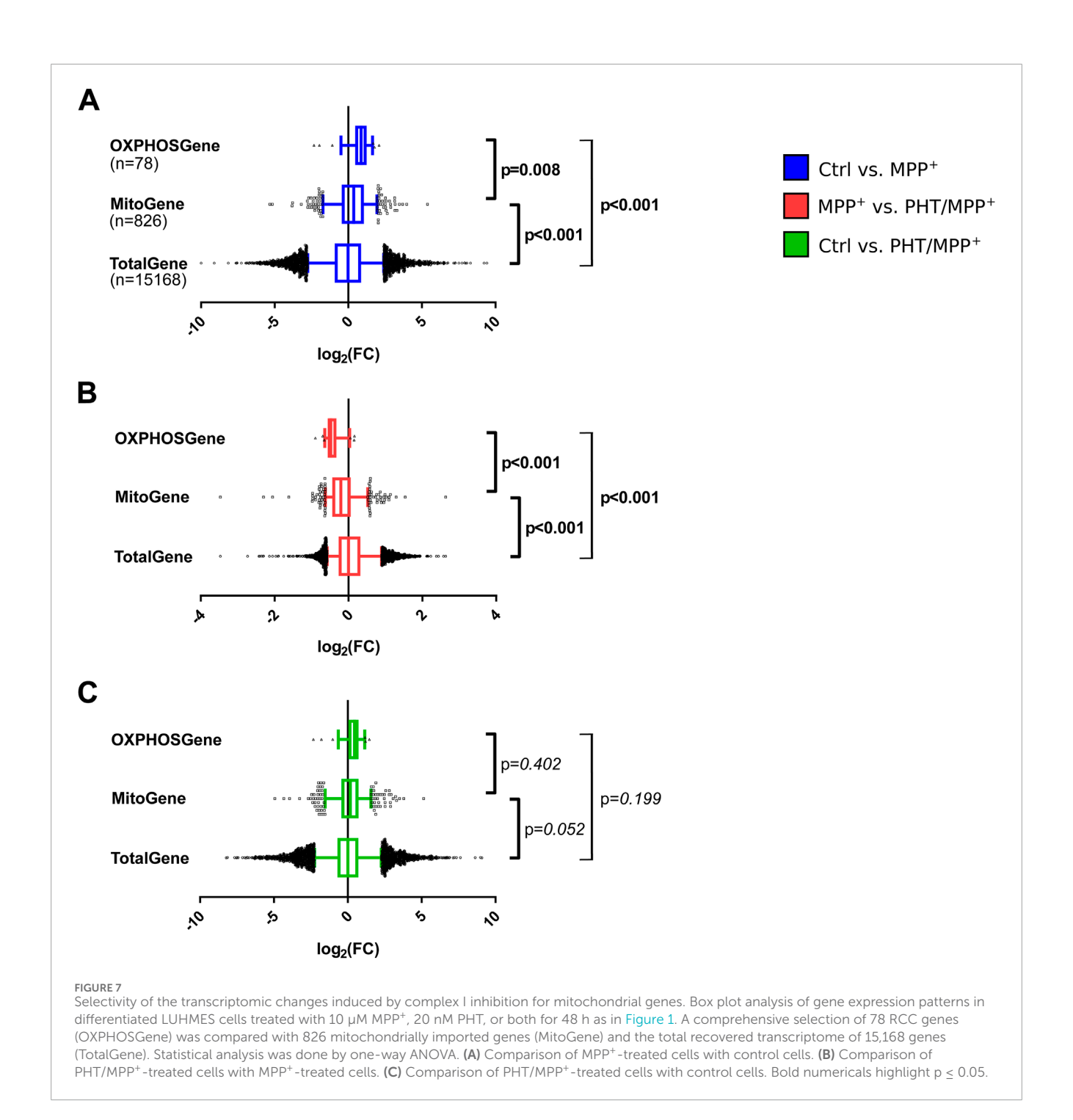


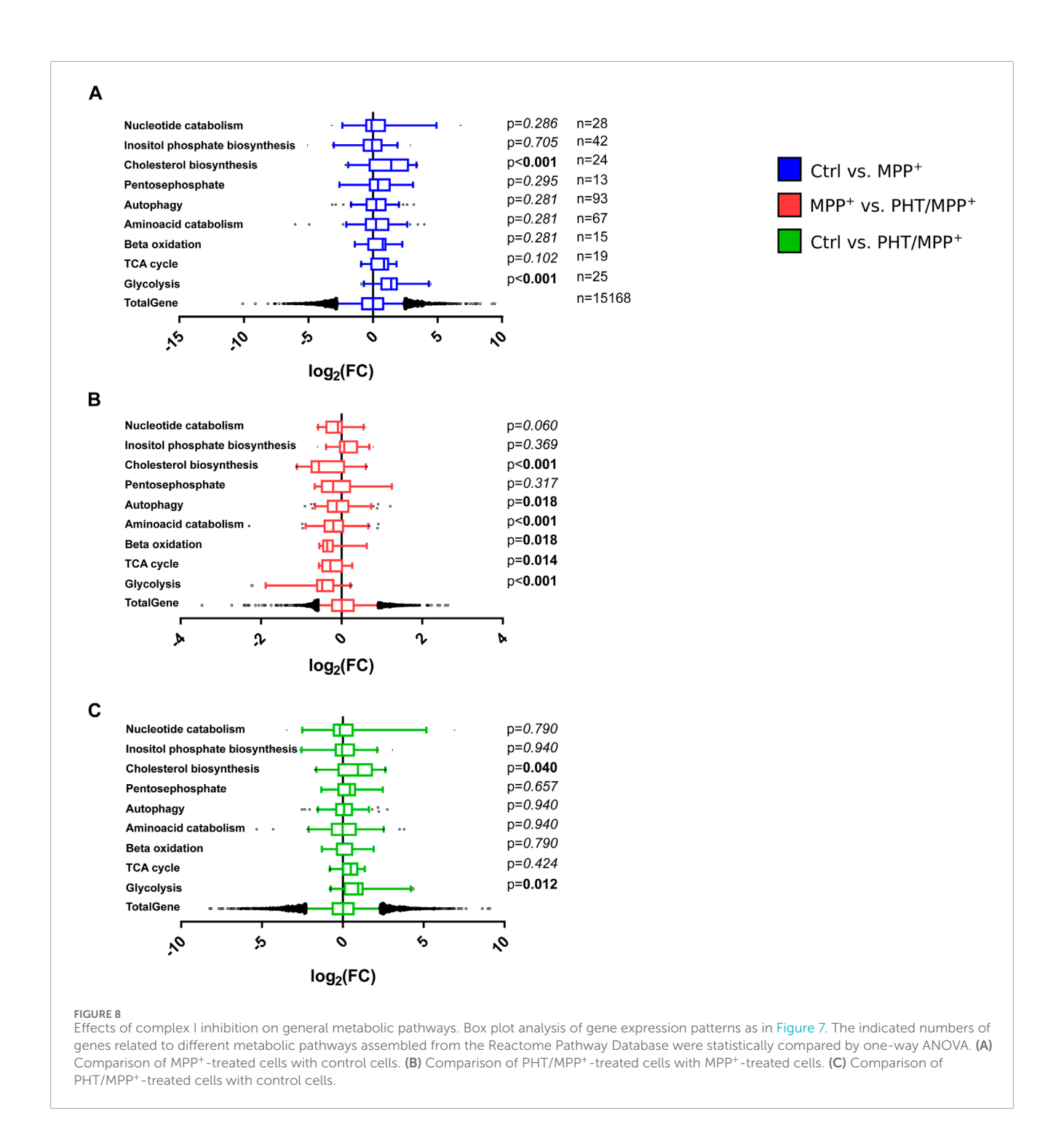
FIGURE 6 Modulation of epigenetic markers by complex I inhibition *in vivo*. **(A)** Immunomicrographs of mouse midbrain slices stained for H3K14ac (red), counterstained with Hoechst 33,258 ('DAPI', blue). DAT dopamine transporter expression is shown in green ('SLC6A3'). Left column: VTA and SN at low magnification; right column: a central area of the SN at high magnification. **(B)** Representative Western blots of midbrain lysates (four mice per group) for H3K14ac, H3, total lysine acetylation, α -tubulin (TUB), SIRT1, SIRT3, SIRT4 and DNMT3B. **(C)** Image analytical quantification of the H3K14ac signal from immunohistochemistry as in A, normalized to total nuclei (n = 9–10 animals, three slices each; number of cells per n: ~1000). **(D)** Densitometric quantification of the H3K14ac signal from Western blotting as in B, normalized to histone H3 expression (n = 9–10 animals). **(E)** The same analysis as in D for total lysine acetylation, normalized to TUB expression (n = 9–10). **(F–I)** Analogous Western blot quantifications of SIRT1, SIRT3, SIRT4 and DNMT3B, all normalized to TUB (n = 9–10).



of PHT lowered mitogenes significantly more than average genes, and RCC complex genes significantly more than other mitogenes (Figure 7B). Notably, the effect of PHT was strong enough to entirely abrogate the differential targeting of mitogenes and RCC complex genes by complex I inhibition (Figure 7C), which suggests that this differential targeting (Figure 7A) was essentially mediated by redox signaling, and not by other mito-nuclear signaling mechanisms (Quiros et al., 2016; Walker and Moraes, 2022).

The above results were compared with an arbitrary selection of other, individually assembled metabolic gene clusters from the Reactome database, as Gene Ontology (GO) term analysis had been inconclusive, failing to return any metabolic clusters

(Supplementary Figure S4). Of nine investigated clusters, two were significantly induced by MPP⁺ treatment, namely, glycolysis and cholesterol biosynthesis (Figure 8A). PHT treatment had a significant suppressive effect on both MPP⁺-induced clusters and, in addition, on several other clusters such as the amino acid catabolism cluster (Figure 8B). In the direct comparison of the control transcriptome with the PHT/MPP⁺ transcriptome, none of the clusters attained significance (Figure 8C) except glycolysis and cholesterol biosynthesis, being modestly induced. These analyses demonstrate that redox signaling was responsible not only for the transcriptional targeting towards the mitochondrion, but also partially responsible for the targeting of glycolysis, a functionally



connected metabolic pathway. The relationship between complex I inhibition and induced cholesterol biosynthesis is elusive, even if a substantial literature exists as regards the potential role of cholesterol in PD (Garcia-Sanz et al., 2021; Al-Kuraishy et al., 2024).

Discussion

Complex I is the main point to entry of electrons into the respiratory chain (Lenaz and Genova, 2009). This also appears to apply to dopaminergic neuronal cells (Risiglione et al., 2020).

Despite its overall high expression in the range of several million copies per cell (Wisniewski et al., 2014), complex I does not seem to be present in large excess, as can be judged from a series of observations. First, patients with severe mitochondrial disease due to complex I mutations still exhibit relatively high residual activities. Affected patients often present with 20%–40% residual activity in muscle biopsies, and 30%–100% residual activity in fibroblasts (Rahman et al., 1996; Kirby et al., 1999; Loeffen et al., 2000; Bugiani et al., 2004), whereas 10%–20% residual activity usually results in lethality (Kirby et al., 1999). Second, despite being the major ubiquinone reductase to fuel complex III and

complex IV in a quasi-linear reaction, it is expressed at a much lower level than the other complexes; specifically, complexes I:III:IV are often expressed at a numeric ratio of approximately 1:3:6 in different tissues and species (Lenaz and Genova, 2009). Moreover, complex I downregulation has emerged as a key adaptation of long-lived animals (Lambert et al., 2010; Munro et al., 2013; Mota-Martorell et al., 2020), suggesting that the exceptionally long-lived *H. sapiens* may also operate at the lowest possible complex I level to avoid reverse electron transport and, thereby, life-shortening ROS overproduction (Mookerjee et al., 2010; Mota-Martorell et al., 2020).

These observations indicate that any incidental losses of complex I activity need to be detected early by the cell, in order to induce compensatory measures, particularly a transcriptional induction of complex I subunits and potentially other RCC subunits in the nucleus. Preferably, such losses should be detected before a severe bioenergetic deficit accrues. In the present study, we show that this is indeed the case in human cells, and we demonstrate that the impending danger signal is an oxidant that can be thwarted by low doses of a radical scavenger. Using a redox signal for this purpose appears to be particularly expedient because oxidant production by certain complex I and III sites is known to be induced rapidly and rather universally in response to diverse pharmacological agents that inhibit RCCs (Tahara et al., 2009; Brand, 2016; Wong et al., 2017). Intriguingly, complex I inhibitors with low toxicity but high antidiabetic efficacy (i.e., metformin versus other bi-/diguanides) appear to be characterized by relatively modest suppression of primary catalysis combined with relatively high induction of superoxide production (Cameron et al., 2018). In fact, the metabolomic and transcriptomic changes elicited by MPP+ and metformin have been shown to be highly overlapping (Abrosimov et al., 2024).

The fact that multiple chemical inhibitors of RCCs cause superoxide production implies that multiple protein damaging events such as denaturation, cofactor loss or lipoxidation will likely evoke the same effect. Hence, impairment of any of the complexes I, III or IV by wear and tear will arguably entail increased superoxide production by either the damaged or an upstream complex. The induced superoxide response is therefore relatively nonspecific because the precise site of damage is not conveyed to the nucleus. However, it is rapid and emanates from the mitochondrion in the wake of a still only functional and perhaps reversible, but not yet structural insufficiency. This aspect is advantageous because there will still be enough ATP to afford protein biosynthesis, and extensive protein damage triggering an unfolded protein response (Zhao et al., 2002; Quiros et al., 2016) is not required to release the signal. After all, there are various types of covalent modifications such as methionine oxidation (Bender et al., 2008; Schindeldecker and Moosmann, 2024) that do not demand immediate repair; only when a specific modification impairs catalysis, a compensatory response is warranted.

The observed transcriptional induction by low-dose MPP⁺ in LUHMES cells was indeed surprisingly uniform as regards the different RCCs (Figure 1). Complex III and IV genes were somewhat more induced than genes related to the actual site of inhibition, complex I (Figure 1). Moreover, glycolytic genes were also selectively induced over a variety of other catabolic and anabolic gene groups (Figure 8), apparently reflecting a purposeful, integrated transcriptional response. The TCA cycle, in contrast, was only marginally modulated, which might be related to the

fact that this pathway conducts epigenetic regulation through its own set of independent signals, namely, succinate, fumarate, and 2hydroxyglutarate (Arnold and Finley, 2023). The induction of the RCCs was reduced by approximately half after application of the radical scavenger PHT, which did not alter any of the MPP+-evoked metabolic changes affecting the pH, lactate, glucose, and NADH as well as the NAD+/NADH ratio (Figure 2). These data support the concept of PHT as a non-pleiotropic, direct radical scavenger (Hajieva et al., 2009; Mocko et al., 2010) that was here employed at a selective 20 nM concentration, which is less than 1/10,000 of its typical toxic dose in cell culture (Moosmann et al., 2001). Notably, ATP levels were unaffected by the employed, 10 μM dose of MPP+, which aligns with the published ATP-modulatory EC₅₀-value of this drug (EC₅₀[ATP] = 65 μ M) (Zhang et al., 2014). It is unclear whether a higher dose of PHT would have effectuated a more pronounced than the observed ~50% reversibility of RCC induction. We would consider this to be well possible, since radical scavengers acting towards short-lived species generally require high concentrations to achieve their maximum effect (Moosmann and Hajieva, 2022). On the other hand, the altered NAD+/NADH ratio may have plausibly contributed to the induction of the compensatory response through sensors like CtBP and, potentially, sirtuins (Anderson et al., 2017).

The chemical identity of the emanated redox signal is unknown at present. Several cues narrow down the set of possible species, though: (i) The signal is scavenged by rather low concentrations of PHT. In view of the established chemistry of PHT and its congeners (Moosmann et al., 2001; Farmer et al., 2017), this points at a radical species and excludes hydrogen peroxide as well as simple diamagnetic electrophiles like aldehydes. (ii) The signal should be closely related to complex I inhibition, which primarily yields superoxide radical anions (Brand, 2016) that are too inert to act as signal themselves (Winterbourn and Hampton, 2008). Still, the signal should be relatable to superoxide. (iii) The signal should be diffusible in the cytosol and potentially reactive enough to directly attack reactive cysteines on DNMT3B and SIRT1, both of which are known to possess such cysteines (Chen et al., 2012; Shao et al., 2014). Still, the signal must not be too reactive, which would limit its diffusion and entail toxicity. This excludes, for instance, hydroxyl radicals. In summary, we propose that perhydroxyl radicals (i.e., protonated superoxide) would fulfill the named requirements best, as they are water soluble (Bielski and Cabelli, 1991), rapidly produced from superoxide in the more acidic cytosol (Saran and Bors, 1994), very reactive with chain-breaking antioxidants mechanistically related to PHT (Bielski and Cabelli, 1991), and of intermediate reactivity with standard cellular compounds like fatty acids and amino acids (Bielski and Shiue, 1978; Bielski et al., 1983). Concomitantly, they exhibit strong selectivity for cysteine when it comes to amino acids (Bielski and Shiue, 1978). Finally, their local production in the cytosol would steeply rise with dropping pH, e.g., in case of cytosolic lactate production (Saran and Bors, 1994), representing a physiologically desirable effect.

The deployment of an epigenetic mechanism to control the collective upregulation of functionally connected household genes (i.e., RCCs) that generally do not require much individual regulation appears expedient and reasonable (Deaton and Bird, 2011). The physically scattered set of genes encoding mitochondrially imported RCC subunits (Supplementary Figure S2) is known to be coregulated as a whole and on the level of the individual complexes,

employing an overlapping set of rather few transcription factors (Lenka et al., 1998; van Waveren and Moraes, 2008). Moreover, RCC subunit genes are generally GC-rich and contain CpG islands in approximately 80% of cases (van Waveren and Moraes, 2008). The specific mechanisms recruited by the proposed redox signal encompass DNA methylation (Figure 3) as well as histone acetylation (Figures 4, 6) and seem to be executed at least in part by DNMT3B and SIRT1. Both players have been linked to PD before: variants in the DNMT3B gene were (softly) associated with sporadic PD in populations from Brazil (Pezzi et al., 2017) and China (Chen et al., 2017). A loss of SIRT1 activity, but not total SIRT activity has been described for cortical tissue samples from patients with PD and other Lewy body diseases (Singh et al., 2017). PDassociated polymorphisms in the SIRT1 gene (Zhang et al., 2012; Maszlag-Török et al., 2021) have also been reported, along with reduced SIRT1 mRNA levels in peripheral blood cells (Maszlag-Török et al., 2021) and reduced SIRT1 protein levels in serum from PD patients (Zhu et al., 2021).

Notably, the use of an epigenetic signal with its inherently limited specificity may also result in adverse off-target effects. For example, we have observed a significant epigenetic activation of LINE1 retrotransposons in LUHMES cells treated with different complex I inhibitors including MPP+ (Baeken et al., 2020). Moreover, the well-established epigenetic induction of SNCA transcription in PD (Jowaed et al., 2010; Matsumoto et al., 2010; Yang et al., 2017) was also recapitulated here (Supplementary Figure S5) and may likewise be classified as adverse and disease-promoting. Inspecting the response of other PD-associated genes (Day and Mullin, 2021) to complex I inhibition, a variety of potentially meaningful effects were observed, some of which were also redox-related. Beyond SNCA, especially PARK2, GBA, PARK7, and ATP13A2 were substantially modulated (Supplementary Figure S5). Of these, the latter two modulations were significantly PHT-reversible, suggesting a redox-epigenetic mechanism of regulation as described herein. On the other hand, PARK2 and GBA were essentially inert to PHT treatment despite being highly induced (PARK2) or repressed (GBA) by MPP+, illustrating the overlap of redox-dependent and redoxindependent mechanisms following complex I inhibition. The strong repression of GBA and ATP13A2 as well as the induction of SNCA also recapitulate the effects of hereditary, PD-causing mutations and duplications, respectively (Lesage and Brice, 2009). Specifically, the known involvement of the GBA protein product (glucocerebrosidase) in α-synuclein degradation (Smith and Schapira, 2022) and the anti-aggregation properties of the ATP13A2 protein towards α-synuclein (Si et al., 2021) indicate that complex I inhibition exerts a triple, arguably synergistic effect towards toxic α-synuclein accumulation (Zharikov et al., 2015) through altered transcriptional regulation.

Conclusion

Complex I-inhibited mitochondria emit an "imminent demand" redox signal to the nucleus, which produces a broad-spectrum transcriptional induction of mito-metabolic genes. The deployed redox signal can be quenched by a one-electron antioxidant, preventing the otherwise evoked loss of DNA

methylation, increase in histone acetylation, and reduction of SIRT1 and nuclear DNMT3B expression. The upregulation of retrotransposons and certain PD-related genes including SNCA following complex I inhibition may constitute inadvertent side-effects of the physiologically purposeful, but pleiotropic induction of mito-metabolic genes via epigenetic chromatin remodeling. The search for the elusive origin of complex I inhibition in PD should be intensified, as it appears to be upstream of the epigenetic alterations in the disease.

Materials and methods

Chemicals and cell culture media

All cell culture media and supplements including Advanced Dulbecco's Modified Eagle's Medium (DMEM)/Ham's F-12 (F12), Phosphate-Buffered Saline (PBS), N2 supplement, Hoechst 33,258, and 6-diamidino-2-phenylindole (DAPI) were obtained from Invitrogen. General laboratory chemicals and biochemicals, neurotoxins, phenothiazine and its derivatives were purchased from Sigma-Aldrich at the highest available purity unless otherwise specified.

Cell culture

LUHMES cells were kindly provided by Dr. Jürgen Winkler (Division of Molecular Neurology, University of Erlangen, Germany). The cells were grown and differentiated as described (Krug et al., 2014; Baeken et al., 2020). At the fourth day post differentiation, the medium was exchanged, and the cells were treated with different compounds at the following concentrations: MPP+: $10 \, \mu M$; PHT: $20 \, nM$; MPHT: $20 \, nM$; APHT: $20 \, nM$; 6-thioguanine: $1 \, \mu M$; EX-257: $100 \, nM$; TSA: $50 \, nM$.

In vivo experiments

In vivo experiments in male C57Bl/6J mice (from Charles River) were performed by QPS Austria GmbH (Grambach, Austria). QPS Austria is accredited by the Association for Assessment and Accreditation of Laboratory Animal Care (AAALAC). Animal care, housing and experimentation were approved by the Institutional Animal Care and Welfare Committee and complied to the animal welfare legislation of the Ministry of Science of the Austrian government.

Thirty mice aged 10 ± 2 weeks were allocated to three different treatment groups: a "vehicle group", an "MPTP group", and an "MPTP plus phenothiazine" group, involving repeated applications or injections of the two agents phenothiazine (10 mg/kg, ten doses *in toto*, vehicle DMSO:corn oil 1:50) and MPTP (20 mg/kg, four doses *in toto*, vehicle saline). The adopted treatment regimen is detailed in Figure 5 and has been described before (Baeken et al, 2020).

Animals from all groups were subjected to the Rotarod motor performance test on day 6 (1 day after the final PHT treatment). Prior to the first test session, the mice were habituated to the testing system until they were able to stay on the rotating rod at a constant

speed of 2 rpm for approximately 1 minute. During testing, a single animal was exposed to the apparatus for three 180 s trials. The initial speed was increased from 2 rpm to 20 rpm during these 180 s. When the mouse fell, the session was over. The mean latency to fall in every single testing was determined.

After finishing the behavioral testing on day 6, the mice were deeply anesthetized by pentobarbital injection (600 mg/kg), transcardially perfused with saline, and dissected. The brains were hemisected, and the left hemisphere was subdivided into striatal tissue, midbrain and residual brain. These samples were rapidly frozen and kept at -80°C until further analysis. The right hemispheres were immersion-fixed in freshly prepared 4% paraformaldehyde in PBS for 1 h at RT. Thereafter, they were transferred to 15% sucrose in PBS until they sank down, indicating sufficient cryoprotection. The hemispheres were cryo-embedded in O.C.T. medium with dry ice-cooled isopentane and afterwards stored at -80°C.

Immunohistochemistry

O.C.T.-embedded brain hemispheres were cut into 10 μ m slices with a cryostat. After washing with PBS, the sections were incubated with 3% BSA/0.1% Triton X-100 in PBS for 1 h at 4°C for blocking and permeabilization. After several washes with PBS, the slices were incubated overnight with primary antibodies at 4°C, repeatedly washed again, and secondary antibodies were applied for 2 h at RT. Following three more washing steps with PBS, 50 ng/mL Hoechst 33,258 was added for 15 min at RT before another PBS wash. Finally, the sections were mounted in anti-fading solution (polyvinyl alcohol/p-phenylendiamine) and stored at -80° C until microscopic evaluation.

The following antibodies were employed: anti-tyrosine hydroxylase (ab112, Abcam, 1:1000 in PBS containing 1% BSA), anti-H3K14ac (7627, Cell Signaling, 1:100), anti-SLC6A3 (DAT) (NBP2-22164, Novus Biologicals, 1:100). Secondary antibodies Cy3-anti-rabbit and Cy2-anti-mouse (Jackson Immunoresearch) were used at 1:1000 dilution for tyrosine hydroxylase, and at 1:200 dilution for SLC6A3 and H3K14ac. All sections were visualized using standard fluorescence microscopy.

Immunocytochemistry

LUHMES cells were plated at 7×10^4 cells/cm² on glass cover slips with standard coating. The experiments were performed on day 6 post differentiation following published protocols (Baeken et al., 2020; Baeken et al., 2021). Cells were incubated with primary antibodies overnight at 4°C and thereupon incubated with secondary antibodies for 2 h at RT. DAPI (1 μ g/mL) was used as nuclear counterstain.

The following primary antibodies were used: anti-acetylated lysine (9441, Cell Signaling, 1:200), anti-DNMT1 (ab13537, Abcam, 1:100), anti-DNMT3A (2160, Cell Signaling, 1:100), anti-DNMT3B (67,259, Cell Signaling, 1:100), anti-5-methylcytosine (28,692, Cell Signaling, 1:200), anti-TUBB (MAB1637, Millipore, 1:500). Cy3-anti-rabbit/Cy2-anti-mouse (Jackson Immunoresearch), 1:400 were used as secondary antibodies.

Microscopy and image analysis

Slides generated through immunohistochemistry were recorded with an Axiovert 200 fluorescence microscope from Zeiss using blue, green and red filters and objectives for ×4 and ×10 magnifications. Immunocytochemistry slides were photographed with a laser scanning microscope (LSM) TCS SP5 from Leica (higher magnifications).

Immunohistochemistry pictures were evaluated using the opensource software ImageJ (imagej.net). Tyrosine hydroxylase (TH) staining was measured after the signal was "watershed": this algorithm calculates signal maxima and thereby allocates cell borders. The cells were quantified using the "analyse particles" function from ImageJ that counts each continuous signal as one particle. Through this approach, cells can be evaluated regardless of the size of their cell body. For H3K14ac staining, total nuclei on the slide were quantified with DAPI, again using the "analyse particle" function of ImageJ. The same process was repeated for the H3K14ac staining, and the quotient H3K14ac/nucleus was calculated. Total acetyl-lysine and 5-methylcytosine levels were also quantified by dividing the intensity measured with ImageJ by the number of cells (nuclei). Stainings of DNMT1, DNMT3A and DNMT3B were evaluated by integration over all z-stacks of the signal intensity that colocalized with DAPI (assigned as "nuclear") or did not colocalize with DAPI (assigned as "cytosolic"). The added signal intensity of both compartments was defined as 100%.

RNA sequencing and bioinformatics

To collect total RNA, LUHMES cells were harvested in 500 µL TRI-Reagent (Sigma-Aldrich) following the manufacturer's instructions

Residual DNA was removed by addition of 2 μL DNAse I (#18047019 from ThermoFisher) and incubation at 37°C for 1 h. Afterwards, 500 μL 75% ethanol were added, and the samples were washed through centrifugation at 7,500 g for 5 min at 4°C. The supernatant was discarded, and the cleaned RNA pellet was reconstituted in 50 μL DEPC-treated H₂O.

The cleaned RNA was analyzed with a 2100 Bioanalyzer from Agilent and quantified using the Qubit dsDNA HS Assay Kit using a Qubit 2.0 Fluorometer (Life Technologies). All nine samples were pooled in equimolar ratio and sequenced in a NextSeq 500 High Output Flowcell with unique adapter sequences, SR for 1×84 cycles, plus 7 cycles for the index read.

Sample demultiplexing and FastQ file generation was performed using Illumina bcl2fastq v2.19.1, and overall sequence quality was assessed with FastQC v.0.11.5. Sequence reads were aligned to the human reference genome GRCh38 with annotation from Gencode release 25 using STAR v.2.5.2b with parameters "--outFilterMismatchNmax 2 --outFilterMultimapNmax 10". Secondary alignments were removed with SAMtools v.1.5, and data quality was examined using RSeQC v2.6.4 and dupRadar v.1.8.0. Read summarization on the gene level was performed using Subread featureCounts v.1.5.1 with stranded option "-s 2". Pairwise differential expression comparisons between sample groups were performed using the Bioconductor package DESeq2 v.1.18.1 using a cutoff of 1% FDR.

Western blot analysis

Whole midbrain tissue and LUHMES cells were homogenized in lysis buffer (50 mM Tris-HCl, pH 6.8; 2% SDS; 10% sucrose; 0.5 mM EDTA; 0.5 mM EGTA plus protease and phosphatase inhibitor cocktails (Sigma-Aldrich)) and were briefly sonicated. Protein concentrations were determined through BCA kit (Pierce) following the manufacturer's protocol. A total of 20 μg protein was loaded onto 12% SDS-PAGE gels and separated with a Mini protean III system (Bio-Rad). The proteins were transferred onto nitrocellulose membranes by electroblotting adopting standard protocols. Following 30 min incubation with 4% low-fat dry milk in PBST, the membranes were incubated with the following primary antibodies: anti-H3K14ac (7627, Cell Signaling, 1:1000), antiacetylated lysine (9441, Cell Signaling, 1:1000), anti-DNMT3B (67,259, Cell Signaling, 1:1000), anti-GLUT3 (ab191071, Abcam, 1:1000), anti-SIRT1 (8469, Cell Signaling, 1:1000), anti-SIRT3 (2627, Cell Signaling, 1:1000), anti-SIRT4 (ab90485, Abcam, 1:1000). Anti- $\alpha\text{-tubulin}$ (T9026, 1:1000, Sigma-Aldrich) and anti-histone H3 (14,269, Cell Signaling, 1:1000) were used as controls for equal protein loading. Primary antibodies were generally detected with horseradish peroxidase-conjugated secondary antibodies (Jackson Immunoresearch). All antibodies used for Western blotting were diluted in PBST. Densitometric analysis of the immunoreactive bands was performed with ImageJ.

Biochemical analyses

ATP, NAD⁺, NADH, glucose and lactate were measured using commercial test kits, following the instructions of the suppliers. Colorimetric or fluorimetric quantifications of the respective readouts were done in a multiwell plate reader (PerkinElmer Wallac Victor 3V) and conducted in white 96-well plates.

For the determination of cellular ATP levels, the medium was aspirated, and the cells were lysed in the supplied buffer. The employed ATP Detection Assay Kit (#700410 from Cayman Chemicals) uses a firefly luciferase system to translate ATP from cell and tissue lysates into luminescence.

NAD+ and NADH measurements were done with the NAD/NADH-Glo Assay Kit (#G9071 from Promega). Cells were grown in 24-well plates, washed, and lysed in 50 μL PBS/50 μL 0.2 M NaOH supplemented with 1% dodecyltrimethylammonium bromide (DTAB). A volume of 50 μL of the lysate was directly heated to 60°C for 15 min (to eliminate NADH), another 50 μL of the lysate were heated to 60°C for 15 min after adding 25 μL 0.4 M HCl (to eliminate NAD+). To stabilize the pH, 25 μL 0.5 M Tris, or 50 μL 0.5 M Tris/HCl were subsequently added to the lysates, respectively. NAD+ and NADH levels were then quantified using the luciferin-coupled, NAD-cycling enzymatic test system provided with the kit.

Glucose and lactate in the medium were determined using the Glucose Colorimetric Assay Kit (#10009582 from Cayman Chemicals) and the Glycolysis Cell-Based Assay Kit (#600450 from Cayman Chemicals), respectively. Prior to analysis, pH values were documented with a calibrated mini-electrode. To avoid interference of phenol red in the medium, a baseline background measurement was performed for each sample. For the lactate measurements, 10 μL medium were used and diluted with water.

MitoChondrial membrane potential was assessed by MitoTracker Red (#M22425 from Invitrogen) staining, followed by microscopic image analysis as described (Hajieva et al., 2009).

ROS levels were determined by quantitative fluorescence microscopy. Cells grown on coverslips were treated as indicated and were incubated with 5 μ M CellROX Deep Red (#C10422 from Invitrogen) for 30 min at 37°C under standard cell culture conditions. Following fixation with 4% PFA and counterstaining with 1 μ g/mL DAPI, fluorescence microscopic images were taken from three separate fields of view with approximately 50 cells per image and analyzed with ImageJ.

Mitochondrial ROS levels were also evaluated with the superoxide-selective dye MitoROS 580 (#ABD-16052 from Biomol). Cells grown and pretreated in 96-well plates as indicated before were incubated with 2x MitoROS 580 working solution in Hank's buffer supplemented with 20 mM HEPES for 30 min at 37°C according to the manufacturer's protocol. Afterwards, the cells were gently washed, and fluorescence intensity was measured with a microplate reader (Tecan Infinite 200 Pro) using 540 nm/590 nm filters.

SIRT1 activity assay

SIRT1 activity in cells lysates was determined with the FLUOR DE LYS SIRT1 fluorometric drug discovery assay kit from Enzo Lifesciences (BML-AK555-0001). In brief, LUHMES cells were harvested in 200 µL SIRT1 assay buffer, briefly sonicated and assessed for protein content with a NanoDrop 1000 photometer. The highest possible amount of protein (181 µg) was diluted in SIRT1 assay buffer to a final volume of $35\,\mu L$ for all samples. Four assay wells per sample were loaded with protein lysate and kept on ice for the remaining procedure. 64 µM SIRT1 substrate, FLUOR DE LYS SIRT1, and 500 μM NAD+ were diluted in 15 μL assay buffer and added to three of the four sample wells. The fourth sample received only 15 µL assay buffer to allow evaluation of the lysate background, while one well only received 50 µL SIRT1 assay buffer, and one well received sample buffer with NAD+ and FLUOR DE LYS SIRT1 to allow quantification of the components' background. The plate was incubated at 37°C for 1 h. The developer solution was prepared with SIRT1 assay buffer, 2 mM nicotinamide to stop additional reactions, and 1x FLUOR DE LYS Developer II. A volume of 50 µL of the developer solution was added to each well except for the background controls, which instead received only 50 µL SIRT1 assay buffer. Two additional wells were prepared, one that only received 50 µL SIRT1 assay buffer and 50 µL developer solution, and one that received 64 µM FLUOR DE LYS Deacetylated Standard (in 50 μL assay buffer) and 50 μL developer solution, to allow for the quantification of the developer solution's background as well as the potential signal maximum. The plate was then incubated at 37°C for 45 min. Afterwards, all fluorescent signals were quantified with a multilabel counter (PerkinElmer Wallac Victor 3V).

Statistical analysis

All data are expressed as mean \pm standard deviation (SD) of the indicated number of independent experiments. Statistically significant differences between the treatment groups were identified

by either one-way or two-way ANOVA as indicated, followed by Benjamini-Hochberg multiple comparisons *post hoc* test. Significance levels are either provided numerically or, in case of the RNA sequencing experiments, coded as symbols denoting $p \le 0.05$.

Data availability statement

The datasets presented in this study can be found in online repositories. The names of the repository/repositories and accession number(s) can be found below: https://www.ncbi.nlm.nih.gov/geo/query/acc.cgi?acc=GSE229460.

Ethics statement

The animal study was approved by the Institutional Animal Care and Welfare Committee of QPS Austria. The study was conducted in accordance with the local legislation and institutional requirements.

Author contributions

MB: Conceptualization, Data curation, Formal Analysis, Investigation, Methodology, Validation, Writing – review and editing, Visualization. AB: Investigation, Methodology, Writing – review and editing. PK: Methodology, Writing – review and editing. CB: Writing – review and editing, Resources. BM: Writing – review and editing, Conceptualization, Data curation, Investigation, Writing – original draft. PH: Conceptualization, Data curation, Investigation, Writing – original draft, Writing – review and editing, Formal Analysis, Funding acquisition, Methodology, Project administration, Supervision, Validation.

Funding

The author(s) declare that financial support was received for the research and/or publication of this article. The study was supported by the Corona Foundation and the Manfred-und-Ursula-Müller Foundation of the "Stifterverband für die Deutsche Wissenschaft", the German Research Council (DFG CRC1177), and the Volkswagen Foundation.

Acknowledgments

The authors thank the team from QPS Austria for their careful planning and excellent realization of the animal experiments. We also thank Michael Plenikowski for the illustrations.

Conflict of interest

The authors declare that the research was conducted in the absence of any commercial or financial relationships that could be construed as a potential conflict of interest.

The author(s) declared that they were an editorial board member of Frontiers, at the time of submission. This had no impact on the peer review process and the final decision.

Generative AI statement

The author(s) declare that no Generative AI was used in the creation of this manuscript.

Publisher's note

All claims expressed in this article are solely those of the authors and do not necessarily represent those of their affiliated organizations, or those of the publisher, the editors and the reviewers. Any product that may be evaluated in this article, or claim that may be made by its manufacturer, is not guaranteed or endorsed by the publisher.

Supplementary material

The Supplementary Material for this article can be found online at: https://www.frontiersin.org/articles/10.3389/fcell.2025. 1608400/full#supplementary-material

SUPPLEMENTARY FIGURE S1

LUHMES morphology. Representative laser scanning microscopic images of differentiated LUHMES cells treated with 10 μ M MPP $^+$ and 20 nM PHT for 48 h (x63 magnification). The neuron-specific β III-tubulin is shown in green, DAPI is shown in blue. The scale bars denote 10 μ m.

SUPPLEMENTARY FIGURE S2

Genomic localization of genes coding for mitochondrially imported RCC subunits. The genomic site of origin of each of the analyzed RCC transcripts (Kent et al., 2002) is indicated using the same color code as in Figure 1 (complex I in red, complex II in blue, complex III in green, complex IV in yellow, complex V in violet).

SUPPLEMENTARY FIGURE S3

Expression of carbonic anhydrases and methionine cycle enzymes. A Transcriptional regulation of all five carbonic anhydrase enzymes detected in LUHMES cells by RNA sequencing. Symbols indicate: $\mbox{\rm *p-value} \le 0.05$ for MPP+ vs. control, $\mbox{\rm #p-value} \le 0.05$ for PHT/MPP+ vs. MPP+. Shading of the fill color is used to denote PHT effects as in Figure 1. B Overview of the methionine cycle. Key enzymes are denoted in blue, indicating their transcriptional modulation (fold change) after MPP+ treatment in brackets. The highlighted enzymes are: methylenetetrahydrofolate reductase (MTHFR), methionine synthase (MTR), methionine adenosyltransferase (MAT2A), adenosylhomocysteine hydrolase (AHCY), cystathionine- $\mbox{\rm F-synthase}$ (CBS). GSH is glutathione. C Bar diagram of the transcriptional modulation by MPP+ and PHT of the five methionine cycle enzymes compiled in B. Symbols and color code are used as in Figure 1.

SUPPLEMENTARY FIGURE \$4

GO analyses. Gene ontology (GO) terms are tabulated that were returned from an unbiased analysis of gene expression changes in LUHMES cells under MPP+ or PHT/MPP+ treatment. The significance cutoff was set at p < 10^{-5} for all comparisons. A GO terms "downregulated" by MPP+ (vs. control). B GO terms "upregulated" by MPP+ (vs. control). C GO terms "downregulated" by PHT (vs. MPP+). D GO terms "upregulated" by PHT (vs. MPP+).

SUPPLEMENTARY FIGURE S5

Transcriptional modulation of Parkinson's disease-related genes by complex I inhibition in LUHMES cells. Regulation of PD-associated genes was measured by RNA sequencing of differentiated LUHMES cells treated with 10 μ M MPP+, 20 nM PHT or both for 48 h as in Figure 1. Transcriptional changes after MPP+ are indicated by bar length; regulation after PHT/MPP+ is indicated by color coding:

lighter color denotes that the MPP⁺ effect was reduced by PHT, darker color denotes that the MPP⁺ effect was increased by PHT. Symbols indicate: *p-value ≤ 0.05 for MPP⁺ vs. control, *p-value ≤ 0.05 for PHT/MPP⁺ vs. MPP⁺ (n = 3, one-way ANOVA). The genes were loosely classified by site and/or function, from top to bottom: lysosomal (red), retrograde transport (pale blue), chaperone (orange), fatty acid metabolism (brown), mitochondrial (blue), synaptic (green).

SUPPLEMENTARY TABLE S1

Chromosomal localization, fold change and statistical significance of the fold change of all genes displayed graphically in this work. The genes are grouped to comprise complex I subunits, complex II subunits, complex IV subunits, complex IV subunits, complex IV subunits, complex IV subunits, mitochondrially encoded RCC subunits, DNA methyltransferases, sirtuins, carbonic anhydrases, methionine cycle enzymes, and Parkinson's disease-related genes.

References

Abrosimov, R., Baeken, M. W., Hauf, S., Wittig, I., Hajieva, P., Perrone, C. E., et al. (2024). Mitochondrial complex I inhibition triggers NAD+-independent glucose oxidation *via* successive NADPH formation, "futile" fatty acid cycling, and FADH2 oxidation. *Geroscience*. 46 (4), 3635–3658. doi:10.1007/s11357-023-01059-y

Agaronyan, K., Morozov, Y. I., Anikin, M., and Temiakov, D. (2015). Mitochondrial biology. Replication-transcription switch in human mitochondria. *Science.* 347 (6221), 548–551. doi:10.1126/science.aaa0986

Agrawal, K., Das, V., Vyas, P., and Hajdúch, M. (2018). Nucleosidic DNA demethylating epigenetic drugs - a comprehensive review from discovery to clinic. *Pharmacol. Ther.* 188, 45–79. doi:10.1016/j.pharmthera.2018.02.006

Alahmad, A., Nasca, A., Heidler, J., Thompson, K., Oláhová, M., Legati, A., et al. (2020). Bi-allelic pathogenic variants in NDUFC2 cause early-onset Leigh syndrome and stalled biogenesis of complex I. *EMBO Mol. Med.* 12 (11), e12619. doi:10.15252/emmm.202012619

Al-Kuraishy, H. M., Fahad, E. H., Al-Windy, S., El-Sherbeni, S. A., Negm, W. A., and Batiha, G. E. (2024). The effects of cholesterol and statins on Parkinson's neuropathology: a narrative review. *Inflammopharmacology* 32 (2), 917–925. doi:10.1007/s10787-023-01400-z

Anderson, K. A., Madsen, A. S., Olsen, C. A., and Hirschey, M. D. (2017). Metabolic control by sirtuins and other enzymes that sense NAD+, NADH, or their ratio. *Biochim. Biophys. Acta Bioenerg.* 1858 (12), 991–998. doi:10.1016/j.bbabio.2017.09.005

Arnold, P. K., and Finley, L. W. S. (2023). Regulation and function of the mammalian tricarboxylic acid cycle. *J. Biol. Chem.* 299 (2), 102838. doi:10.1016/j.jbc.2022.102838

Atamna, H., Nguyen, A., Schultz, C., Boyle, K., Newberry, J., Kato, H., et al. (2008). Methylene blue delays cellular senescence and enhances key mitochondrial biochemical pathways. *FASEB J.* 22 (3), 703–712. doi:10.1096/fj.07-9610com

Baeken, M. W. (2024). Sirtuins and their influence on autophagy. J. Cell Biochem. 125 (11), e30377. doi:10.1002/jcb.30377

Baeken, M. W., Moosmann, B., and Hajieva, P. (2020). Retrotransposon activation by distressed mitochondria in neurons. *Biochem. Biophys. Res. Commun.* 525 (3), 570–575. doi:10.1016/j.bbrc.2020.02.106

Baeken, M. W., Schwarz, M., Kern, A., Moosmann, B., Hajieva, P., and Behl, C. (2021). The selective degradation of sirtuins via macroautophagy in the MPP+ model of Parkinson's disease is promoted by conserved oxidation sites. *Cell Death Discov.* 7 (1), 286. doi:10.1038/s41420-021-00683-x

Beal, M. F. (2001). Experimental models of Parkinson's disease. *Nat. Rev. Neurosci.* 2 (5), 325–334. doi:10.1038/35072550

Belogrudov, G. I. (2009). Recent advances in structure-functional studies of mitochondrial factor B. *J. Bioenerg. Biomembr.* 41 (2), 137–143. doi:10.1007/s10863-009-9210-1

Bender, A., Hajieva, P., and Moosmann, B. (2008). Adaptive antioxidant methionine accumulation in respiratory chain complexes explains the use of a deviant genetic code in mitochondria. *Proc. Natl. Acad. Sci. U. S. A.* 105 (43), 16496–16501. doi:10.1073/pnas.0802779105

Betarbet, R., Sherer, T. B., MacKenzie, G., Garcia-Osuna, M., Panov, A. V., and Greenamyre, J. T. (2000). Chronic systemic pesticide exposure reproduces features of Parkinson's disease. *Nat. Neurosci.* 3 (12), 1301–1306. doi:10.1038/81834

Bielski, B. H., Arudi, R. L., and Sutherland, M. W. (1983). A study of the reactivity of HO2/O2- with unsaturated fatty acids. *J. Biol. Chem.* 258 (8), 4759–4761. doi:10.1016/s0021-9258(18)32488-8

Bielski, B. H., and Cabelli, D. E. (1991). Highlights of current research involving superoxide and perhydroxyl radicals in aqueous solutions. *Int. J. Radiat. Biol.* 59 (2), 291–319. doi:10.1080/09553009114550301

Bielski, B. H., and Shiue, G. G. (1978). Reaction rates of superoxide radicals with the essential amino acids, Ciba Found. Symp. 65, 43-56. doi:10.1002/9780470715413.ch4

Brand, M. D. (2016). Mitochondrial generation of superoxide and hydrogen peroxide as the source of mitochondrial redox signaling. *Free Radic. Biol. Med.* 100, 14–31. doi:10.1016/j.freeradbiomed.2016.04.001

Bugiani, M., Invernizzi, F., Alberio, S., Briem, E., Lamantea, E., Carrara, F., et al. (2004). Clinical and molecular findings in children with complex I deficiency. *Biochim. Biophys. Acta* 1659 (2-3), 136–147. doi:10.1016/j.bbabio.2004.09.006

Cameron, A. R., Logie, L., Patel, K., Erhardt, S., Bacon, S., Middleton, P., et al. (2018). Metformin selectively targets redox control of complex I energy transduction. *Redox Biol.* 14, 187–197. doi:10.1016/j.redox.2017.08.018

Cannon, J. R., and Greenamyre, J. T. (2011). The role of environmental exposures in neurodegeneration and neurodegenerative diseases. *Toxicol. Sci.* 124 (2), 225–250. doi:10.1093/toxsci/kfr239

Cannon, J. R., Tapias, V., Na, H. M., Honick, A. S., Drolet, R. E., and Greenamyre, J. T. (2009). A highly reproducible rotenone model of Parkinson's disease. *Neurobiol. Dis.* 34 (2), 279–290. doi:10.1016/j.nbd.2009.01.016

Chen, C. C., Wang, K. Y., and Shen, C. K. (2012). The mammalian *de novo* DNA methyltransferases DNMT3A and DNMT3B are also DNA 5-hydroxymethylcytosine dehydroxymethylases. *J. Biol. Chem.* 287 (40), 33116–33121. doi:10.1074/jbc.C112.406975

Chen, X., Xiao, Y., Wei, L., Wu, Y., Lu, J., Guo, W., et al. (2017). Association of DNMT3b gene variants with sporadic Parkinson's disease in a Chinese Han population. *J. Gene Med.* 19 (11), 360–365. doi:10.1002/jgm.2991

Chen, Y., and Shen, Y. Q. (2025). Role of reactive oxygen species in regulating epigenetic modifications. *Cell Signal* 125, 111502. doi:10.1016/j.cellsig.2024.111502

Chia, S. J., Tan, E. K., and Chao, Y. X. (2020). Historical perspective: models of Parkinson's disease. *Int. J. Mol. Sci.* 21 (7), 2464. doi:10.3390/ijms21072464

Creed, R. B., and Goldberg, M. S. (2018). New developments in genetic rat models of Parkinson's disease. *Mov. Disord.* 33 (5), 717–729. doi:10.1002/mds.27296

Dawson, T. M., Ko, H. S., and Dawson, V. L. (2010). Genetic animal models of Parkinson's disease. *Neuron* 66 (5), 646–661. doi:10.1016/j.neuron.2010.04.034

Day, J. O., and Mullin, S. (2021). The genetics of Parkinson's disease and implications for clinical practice. *Genes (Basel)* 12 (7), 1006. doi:10.3390/genes12071006

Deaton, A. M., and Bird, A. (2011). CpG islands and the regulation of transcription. Genes Dev. 25 (10), 1010-1022. doi:10.1101/gad.2037511

Desplats, P., Spencer, B., Coffee, E., Patel, P., Michael, S., Patrick, C., et al. (2011). Alpha-synuclein sequesters Dnmt1 from the nucleus: a novel mechanism for epigenetic alterations in Lewy body diseases. *J. Biol. Chem.* 286 (11), 9031–9037. doi:10.1074/jbc.C110.212589

Du, Z., Song, J., Wang, Y., Zhao, Y., Guda, K., Yang, S., et al. (2010). DNMT1 stability is regulated by proteins coordinating deubiquitination and acetylation-driven ubiquitination. *Sci. Signal* 3 (146), ra80. doi:10.1126/scisignal.2001462

Elkholi, R., Abraham-Enachescu, I., Trotta, A. P., Rubio-Patiño, C., Mohammed, J. N., Luna-Vargas, M. P. A., et al. (2019). MDM2 integrates cellular respiration and apoptotic signaling through NDUFS1 and the mitochondrial network. *Mol. Cell* 74 (3), 452–465.e7. doi:10.1016/j.molcel.2019.02.012

Fallon, J., Matthews, R. T., Hyman, B. T., and Beal, M. F. (1997). MPP+ produces progressive neuronal degeneration which is mediated by oxidative stress. *Exp. Neurol.* 144 (1), 193–198. doi:10.1006/exnr.1997.6416

Farmer, L. A., Haidasz, E. A., Griesser, M., and Pratt, D. A. (2017). Phenoxazine: a privileged scaffold for radical-trapping antioxidants. *J. Org. Chem.* 82 (19), 10523–10536. doi:10.1021/acs.joc.7b02025

Feng, Y., Liu, T., Dong, S. Y., Guo, Y. J., Jankovic, J., Xu, H., et al. (2015). Rotenone affects p53 transcriptional activity and apoptosis *via* targeting SIRT1 and H3K9 acetylation in SH-SY5Y cells. *J. Neurochem.* 134 (4), 668–676. doi:10.1111/jnc.13172

Flones, I. H., Fernandez-Vizarra, E., Lykouri, M., Brakedal, B., Skeie, G. O., Miletic, H., et al. (2018). Neuronal complex I deficiency occurs throughout the Parkinson's disease brain, but is not associated with neurodegeneration or mitochondrial DNA damage. *Acta Neuropathol.* 135 (3), 409–425. doi:10.1007/s00401-017-1794-7

Garcia-Sanz, P., M, F. G., Aerts, J., and Moratalla, R. (2021). The role of cholesterol in α -synuclein and Lewy body pathology in GBA1 Parkinson's disease. *Mov. Disord.* 36 (5), 1070–1085. doi:10.1002/mds.28396

Gatt, A. P., Duncan, O. F., Attems, J., Francis, P. T., Ballard, C. G., and Bateman, J. M. (2016). Dementia in Parkinson's disease is associated with enhanced mitochondrial complex I deficiency. *Mov. Disord.* 31 (3), 352–359. doi:10.1002/mds.26513

Gebremedhin, K. G., and Rademacher, D. J. (2016). Histone H3 acetylation in the postmortem Parkinson's disease primary motor cortex. *Neurosci. Lett.* 627, 121–125. doi:10.1016/j.neulet.2016.05.060

Gibrat, C., Saint-Pierre, M., Bousquet, M., Lévesque, D., Rouillard, C., and Cicchetti, F. (2009). Differences between subacute and chronic MPTP mice models: investigation of dopaminergic neuronal degeneration and alpha-synuclein inclusions. *J. Neurochem.* 109 (5), 1469–1482. doi:10.1111/j.1471-4159.2009.06072.x

Hajieva, P., Mocko, J. B., Moosmann, B., and Behl, C. (2009). Novel imine antioxidants at low nanomolar concentrations protect dopaminergic cells from oxidative neurotoxicity. *J. Neurochem.* 110 (1), 118–132. doi:10.1111/j.1471-4159.2009.06114.x

Harrison, I. F., Smith, A. D., and Dexter, D. T. (2018). Pathological histone acetylation in Parkinson's disease: neuroprotection and inhibition of microglial activation through SIRT 2 inhibition. *Neurosci. Lett.* 666, 48–57. doi:10.1016/j.neulet.2017.12.037

Hermann, A., Gowher, H., and Jeltsch, A. (2004). Biochemistry and biology of mammalian DNA methyltransferases. *Cell Mol. Life Sci.* 61 (19-20), 2571–2587. doi:10.1007/s00018-004-4201-1

Huang, Y. H., Chen, C. W., Sundaramurthy, V., Słabicki, M., Hao, D., Watson, C. J., et al. (2022). Systematic profiling of DNMT3A variants reveals protein instability mediated by the DCAF8 E3 ubiquitin ligase adaptor. *Cancer Discov.* 12 (1), 220–235. doi:10.1158/2159-8290.CD-21-0560

Johannessen, J. N., Adams, J. D., Schuller, H. M., Bacon, J. P., and Markey, S. P. (1986). 1-Methyl-4-phenylpyridine (MPP+) induces oxidative stress in the rodent. *Life Sci.* 38 (8), 743–749. doi:10.1016/0024-3205(86)90589-8

Jowaed, A., Schmitt, I., Kaut, O., and Wüllner, U. (2010). Methylation regulates alphasynuclein expression and is decreased in Parkinson's disease patients' brains. *J. Neurosci.* 30 (18), 6355–6359. doi:10.1523/JNEUROSCI.6119-09.2010

Kalous, K. S., Wynia-Smith, S. L., Summers, S. B., and Smith, B. C. (2020). Human sirtuins are differentially sensitive to inhibition by nitrosating agents and other cysteine oxidants. *J. Biol. Chem.* 295 (25), 8524–8536. doi:10.1074/jbc.RA119.011988

Karmodiya, K., Krebs, A. R., Oulad-Abdelghani, M., Kimura, H., and Tora, L. (2012). H3K9 and H3K14 acetylation co-occur at many gene regulatory elements, while H3K14ac marks a subset of inactive inducible promoters in mouse embryonic stem cells. *BMC Genomics* 13, 424. doi:10.1186/1471-2164-13-424

Kaut, O., Schmitt, I., Stahl, F., Fröhlich, H., Hoffmann, P., Gonzalez, F. J., et al. (2022). Epigenome-wide analysis of DNA methylation in Parkinson's disease cortex. *Life (Basel)* 12 (4), 502. doi:10.3390/life12040502

Keeney, P. M., Xie, J., Capaldi, R. A., and Bennett, J. P., Jr (2006). Parkinson's disease brain mitochondrial complex I has oxidatively damaged subunits and is functionally impaired and misassembled. *J. Neurosci.* 26 (19), 5256–5264. doi:10.1523/JNEUROSCI.0984-06.2006

Kent, W. J., Sugnet, C. W., Furey, T. S., Roskin, K. M., Pringle, T. H., Zahler, A. M., et al. (2002). The human genome browser at UCSC. *Genome Res.* 12 (6), 996–1006. doi:10.1101/gr.229102

Kidd, S. K., and Schneider, J. S. (2010). Protection of dopaminergic cells from MPP+-mediated toxicity by histone deacetylase inhibition. *Brain Res.* 1354, 172–178. doi:10.1016/j.brainres.2010.07.041

Kirby, D. M., Crawford, M., Cleary, M. A., Dahl, H. H., Dennett, X., and Thorburn, D. R. (1999). Respiratory chain complex I deficiency: an underdiagnosed energy generation disorder. *Neurology* 52 (6), 1255–1264. doi:10.1212/wnl.52.6.1255

Krug, A. K., Gutbier, S., Zhao, L., Pöltl, D., Kullmann, C., Ivanova, V., et al. (2014). Transcriptional and metabolic adaptation of human neurons to the mitochondrial toxicant MPP(+). *Cell Death Dis.* 5 (5), e1222. doi:10.1038/cddis.2014.166

Kunath, S., Schindeldecker, M., De Giacomo, A., Meyer, T., Sohre, S., Hajieva, P., et al. (2020). Prooxidative chain transfer activity by thiol groups in biological systems. *Redox Biol.* 36, 101628. doi:10.1016/j.redox.2020.101628

Lambert, A. J., Buckingham, J. A., Boysen, H. M., and Brand, M. D. (2010). Low complex I content explains the low hydrogen peroxide production rate of heart mitochondria from the long-lived pigeon, Columba livia. *Aging Cell* 9 (1), 78–91. doi:10.1111/j.1474-9726.2009.00538.x

Langston, J. W. (2017). The MPTP story. J. Park. Dis. 7 (s1), S11–S19. doi:10.3233/JPD-179006

Langston, J. W., Ballard, P., Tetrud, J. W., and Irwin, I. (1983). Chronic Parkinsonism in humans due to a product of meperidine-analog synthesis. *Science* 219 (4587), 979–980. doi:10.1126/science.6823561

Lenaz, G., and Genova, M. L. (2009). Structural and functional organization of the mitochondrial respiratory chain: a dynamic super-assembly. *Int. J. Biochem. Cell Biol.* 41 (10), 1750–1772. doi:10.1016/j.biocel.2009.04.003

Lenka, N., Vijayasarathy, C., Mullick, J., and Avadhani, N. G. (1998). Structural organization and transcription regulation of nuclear genes encoding the mammalian cytochrome c oxidase complex. *Prog. Nucleic Acid. Res. Mol. Biol.* 61, 309–344. doi:10.1016/s0079-6603(08)60830-2

Lesage, S., and Brice, A. (2009). Parkinson's disease: from monogenic forms to genetic susceptibility factors. *Hum. Mol. Genet.* 18 (R1), R48–R59. doi:10.1093/hmg/ddp012

Loeffen, J. L., Smeitink, J. A., Trijbels, J. M., Janssen, A. J., Triepels, R. H., Sengers, R. C., et al. (2000). Isolated complex I deficiency in children: clinical, biochemical and genetic aspects. *Hum. Mutat.* 15 (2), 123–134. doi:10.1002/(SICI)1098-1004(200002)15:2<123::AID-HUMU1>3.0.CO;2-P

Masliah, E., Dumaop, W., Galasko, D., and Desplats, P. (2013). Distinctive patterns of DNA methylation associated with Parkinson disease: identification of concordant epigenetic changes in brain and peripheral blood leukocytes. *Epigenetics* 8 (10), 1030–1038. doi:10.4161/epi.25865

Maszlag-Török, R., Boros, F. A., Vécsei, L., and Klivényi, P. (2021). Gene variants and expression changes of SIRT1 and SIRT6 in peripheral blood are associated with Parkinson's disease. *Sci Rep.* 11 (1), 10677. doi:10.1038/s41598-021-90059-z

Matsumoto, L., Takuma, H., Tamaoka, A., Kurisaki, H., Date, H., Tsuji, S., et al. (2010). CpG demethylation enhances alpha-synuclein expression and affects the pathogenesis of Parkinson's disease. *PLoS One* 5 (11), e15522. doi:10.1371/journal.pone.0015522

Mender, I., Gryaznov, S., Dikmen, Z. G., Wright, W. E., and Shay, J. W. (2015). Induction of telomere dysfunction mediated by the telomerase substrate precursor 6-thio-2'-deoxyguanosine. *Cancer Discov.* 5 (1), 82–95. doi:10.1158/2159-8290.CD-14-0609

Mocko, J. B., Kern, A., Moosmann, B., Behl, C., and Hajieva, P. (2010). Phenothiazines interfere with dopaminergic neurodegeneration in *Caenorhabditis elegans* models of Parkinson's disease. *Neurobiol. Dis.* 40 (1), 120–129. doi:10.1016/j.nbd.2010.03.019

Mookerjee, S. A., Divakaruni, A. S., Jastroch, M., and Brand, M. D. (2010). Mitochondrial uncoupling and lifespan. *Mech. Ageing Dev.* 131 (7-8), 463–472. doi:10.1016/j.mad.2010.03.010

Moosmann, B., and Behl, C. (2002). Antioxidants as treatment for neurodegenerative disorders. *Expert Opin. Investig. Drugs* 11 (10), 1407–1435. doi:10.1517/13543784.11.10.1407

Moosmann, B., and Hajieva, P. (2022). Probing the role of cysteine thiyl radicals in biology: eminently dangerous, difficult to scavenge. *Antioxidants (Basel)* 11 (5), 885. doi:10.3390/antiox11050885

Moosmann, B., Skutella, T., Beyer, K., and Behl, C. (2001). Protective activity of aromatic amines and imines against oxidative nerve cell death. *Biol. Chem.* 382 (11), 1601–1612. doi:10.1515/BC.2001.195

Mota-Martorell, N., Jove, M., Pradas, I., Sanchez, I., Gómez, J., Naudi, A., et al. (2020). Low abundance of NDUFV2 and NDUFS4 subunits of the hydrophilic complex I domain and VDAC1 predicts mammalian longevity. *Redox Biol.* 34, 101539. doi:10.1016/j.redox.2020.101539

Munro, D., Pichaud, N., Paquin, F., Kemeid, V., and Blier, P. U. (2013). Low hydrogen peroxide production in mitochondria of the long-lived arctica islandica: underlying mechanisms for slow aging. *Aging Cell* 12 (4), 584–592. doi:10.1111/acel.12082

Napper, A. D., Hixon, J., McDonagh, T., Keavey, K., Pons, J. F., Barker, J., et al. (2005). Discovery of indoles as potent and selective inhibitors of the deacetylase SIRT1. *J. Med. Chem.* 48 (25), 8045–8054. doi:10.1021/jm050522v

Ohlow, M. J., and Moosmann, B. (2011). Phenothiazine: the seven lives of pharmacology's first lead structure. *Drug Discov. Today* 16 (3-4), 119–131. doi:10.1016/j.drudis.2011.01.001

Park, G., Tan, J., Garcia, G., Kang, Y., Salvesen, G., and Zhang, Z. (2016). Regulation of histone acetylation by autophagy in Parkinson disease. *J. Biol. Chem.* 291 (7), 3531–3540. doi:10.1074/jbc.M115.675488

Pezzi, J. C., de Bem, C. M., da Rocha, T. J., Schumacher-Schuh, A. F., Chaves, M. L., Rieder, C. R., et al. (2017). Association between DNA methyltransferase gene polymorphism and Parkinson's disease. *Neurosci. Lett.* 639, 146–150. doi:10.1016/j.neulet.2016.12.058

Quiros, P. M., Mottis, A., and Auwerx, J. (2016). Mitonuclear communication in homeostasis and stress. *Nat. Rev. Mol. Cell Biol.* 17 (4), 213–226. doi:10.1038/nrm.2016.23

Rahman, S., Blok, R. B., Dahl, H. H., Danks, D. M., Kirby, D. M., Chow, C. W., et al. (1996). Leigh syndrome: clinical features and biochemical and DNA abnormalities. Ann. Neurol. 39 (3), 343–351. doi:10.1002/ana.410390311

Ramsay, R. R., Kowal, A. T., Johnson, M. K., Salach, J. I., and Singer, T. P. (1987). The inhibition site of MPP+, the neurotoxic bioactivation product of 1-methyl-4-phenyl-1,2,3,6-tetrahydropyridine is near the Q-binding site of NADH dehydrogenase. *Arch. Biochem. Biophys.* 259 (2), 645–649. doi:10.1016/0003-9861(87)90531-5

Richardson, J. R., Quan, Y., Sherer, T. B., Greenamyre, J. T., and Miller, G. W. (2005). Paraquat neurotoxicity is distinct from that of MPTP and rotenone. *Toxicol. Sci.* 88 (1), 193–201. doi:10.1093/toxsci/kfi304

Risiglione, P., Leggio, L., Cubisino, S. A. M., Reina, S., Paternò, G., Marchetti, B., et al. (2020). High-resolution respirometry reveals MPP+ mitochondrial toxicity mechanism in a cellular model of Parkinson's disease. *Int. J. Mol. Sci.* 21 (21), 7809. doi:10.3390/iims21217809

Saran, M., and Bors, W. (1994). Signalling by O2-. and NO.: how far can either radical, or any specific reaction product, transmit a message under *in vivo* conditions? *Chem. Biol. Interact.* 90 (1), 35–45. doi:10.1016/0009-2797(94)90109-0

Sayre, L. M., Perry, G., and Smith, M. A. (2008). Oxidative stress and neurotoxicity. Chem. Res. Toxicol. 21 (1), 172–188. doi:10.1021/tx700210j

Schaffner, S. L., and Kobor, M. S. (2022). DNA methylation as a mediator of genetic and environmental influences on Parkinson's disease susceptibility: impacts of alphasynuclein, physical activity, and pesticide exposure on the epigenome. *Front. Genet.* 13, 971298. doi:10.3389/fgene.2022.971298

Schapira, A. H., Cooper, J. M., Dexter, D., Clark, J. B., Jenner, P., and Marsden, C. D. (1990). Mitochondrial complex I deficiency in Parkinson's disease. *J. Neurochem.* 54 (3), 823–827. doi:10.1111/j.1471-4159.1990.tb02325.x

- Schindeldecker, M., and Moosmann, B. (2024). Cysteine is the only universally affected and disfavored proteomic amino acid under oxidative conditions in animals. *Antioxidants (Basel)* 13 (3), 267. doi:10.3390/antiox13030267
- Shao, D., Fry, J. L., Han, J., Hou, X., Pimentel, D. R., Matsui, R., et al. (2014). A redox-resistant sirtuin-1 mutant protects against hepatic metabolic and oxidant stress. *J. Biol. Chem.* 289 (11), 7293–7306. doi:10.1074/jbc.M113.520403
- Sherer, T. B., Richardson, J. R., Testa, C. M., Seo, B. B., Panov, A. V., Yagi, T., et al. (2007). Mechanism of toxicity of pesticides acting at complex I: relevance to environmental etiologies of Parkinson's disease. *J. Neurochem.* 100 (6), 1469–1479. doi:10.1111/j.1471-4159.2006.04333.x
- Si, J., Van den Haute, C., Lobbestael, E., Martin, S., van Veen, S., Vangheluwe, P., et al. (2021). ATP13A2 regulates cellular α -synuclein multimerization, membrane association, and externalization. *Int. J. Mol. Sci.* 22 (5), 2689. doi:10.3390/iims22052689
- Singh, P., Hanson, P. S., and Morris, C. M. (2017). SIRT1 ameliorates oxidative stress induced neural cell death and is down-regulated in Parkinson's disease. *BMC Neurosci.* 18 (1), 46. doi:10.1186/s12868-017-0364-1
- Smirnova, L., Harris, G., Delp, J., Valadares, M., Pamies, D., Hogberg, H. T., et al. (2016). A LUHMES 3D dopaminergic neuronal model for neurotoxicity testing allowing long-term exposure and cellular resilience analysis. *Arch. Toxicol.* 90 (11), 2725–2743. doi:10.1007/s00204-015-1637-z
- Smith, L., and Schapira, A. H. V. (2022). GBA variants and Parkinson disease: mechanisms and treatments. *Cells* 11 (8), 1261. doi:10.3390/cells11081261
- Swerdlow, R. H. (2020). The mitochondrial hypothesis: dysfunction, bioenergetic defects, and the metabolic link to Alzheimer's disease. *Int. Rev. Neurobiol.* 154, 207–233. doi:10.1016/bs.irn.2020.01.008
- Tahara, E. B., Navarete, F. D., and Kowaltowski, A. J. (2009). Tissue-substrateand site-specific characteristics of mitochondrial reactive oxygen species generation. *Free Radic. Biol. Med.* 46 (9), 1283–1297. doi:10.1016/j.freeradbiomed. 2009.02.008
- Tapias, V., McCoy, J. L., and Greenamyre, T. J. (2019). Phenothiazine normalizes the NADH/NAD+ ratio, maintains mitochondrial integrity and protects the nigrostriatal dopamine system in a chronic rotenone model of Parkinson's disease. *Redox Biol.* 24, 101164. doi:10.1016/j.redox.2019.101164
- Terada, T., Therriault, J., Kang, M. S. P., Savard, M., Pascoal, T. A., Lussier, F., et al. (2021). Mitochondrial complex I abnormalities is associated with tau and clinical symptoms in mild Alzheimer's disease. *Mol. Neurodegener.* 16 (1), 28. doi:10.1186/s13024-021-00448-1
- Toker, L., Tran, G. T., Sundaresan, J., Tysnes, O. B., Alves, G., Haugarvoll, K., et al. (2021). Genome-wide histone acetylation analysis reveals altered transcriptional regulation in the Parkinson's disease brain. *Mol. Neurodegener.* 16 (1), 31. doi:10.1186/s13024-021-00450-7

- van Waveren, C., and Moraes, C. T. (2008). Transcriptional co-expression and coregulation of genes coding for components of the oxidative phosphorylation system. BMC Genomics 9, 18. doi:10.1186/1471-2164-9-18
- Walker, B. R., and Moraes, C. T. (2022). Nuclear-mitochondrial interactions. *Biomolecules* 12 (3), 427. doi:10.3390/biom12030427
- Winterbourn, C. C., and Hampton, M. B. (2008). Thiol chemistry and specificity in redox signaling. *Free Radic. Biol. Med.* 45 (5), 549–561. doi:10.1016/j.freeradbiomed.2008.05.004
- Wisniewski, J. R., Hein, M. Y., Cox, J., and Mann, M. (2014). A "proteomic ruler" for protein copy number and concentration estimation without spike-in standards. *Mol. Cell Proteomics* 13 (12), 3497–3506. doi:10.1074/mcp.M113.037309
- Wong, H. S., Dighe, P. A., Mezera, V., Monternier, P. A., and Brand, M. D. (2017). Production of superoxide and hydrogen peroxide from specific mitochondrial sites under different bioenergetic conditions. *J. Biol. Chem.* 292 (41), 16804–16809. doi:10.1074/jbc.R117.789271
- Yang, J., Yang, Z., Wang, X., Sun, M., Wang, Y., and Wang, X. (2017). CpG demethylation in the neurotoxicity of 1-methyl-4-phenylpyridinium might mediate transcriptional up-regulation of α -synuclein in SH-SY5Y cells. *Neurosci. Lett.* 659, 124–132. doi:10.1016/j.neulet.2017.08.023
- Yoshida, M., Kijima, M., Akita, M., and Beppu, T. (1990). Potent and specific inhibition of mammalian histone deacetylase both *in vivo* and *in vitro* by trichostatin A. *J. Biol. Chem.* 265, 17174–17179. doi:10.1016/s0021-9258(17)44885-x
- Yuan, B., Zhang, J., Wang, H., Xiong, L., Cai, Q., Wang, T., et al. (2011). 6-Thioguanine reactivates epigenetically silenced genes in acute lymphoblastic leukemia cells by facilitating proteasome-mediated degradation of DNMT1. *Cancer Res.* 71 (5), 1904–1911. doi:10.1158/0008-5472.CAN-10-3430
- Zeng, X. S., Geng, W. S., and Jia, J. J. (2018). Neurotoxin-induced animal models of Parkinson disease: pathogenic mechanism and assessment. *ASN Neuro* 10, 1759091418777438. doi:10.1177/1759091418777438
- Zhang, A., Wang, H., Qin, X., Pang, S., and Yan, B. (2012). Genetic analysis of SIRT1 gene promoter in sporadic Parkinson's disease. *Biochem. Biophys. Res. Commun.* 422 (4), 693–696. doi:10.1016/j.bbrc.2012.05.059
- Zhang, X. M., Yin, M., and Zhang, M. H. (2014). Cell-based assays for Parkinson's disease using differentiated human LUHMES cells. *Acta Pharmacol. Sin.* 35 (7), 945–956. doi:10.1038/aps.2014.36
- Zhao, Q., Wang, J., Levichkin, I. V., Stasinopoulos, S., Ryan, M. T., and Hoogenraad, N. J. (2002). A mitochondrial specific stress response in mammalian cells. *EMBO J.* 21 (17), 4411–4419. doi:10.1093/emboj/cdf445
- Zharikov, A. D., Cannon, J. R., Tapias, V., Bai, Q., Horowitz, M. P., Shah, V., et al. (2015). shRNA targeting α -synuclein prevents neurodegeneration in a Parkinson's disease model. *J. Clin. Invest* 125 (7), 2721–2735. doi:10.1172/JCI64502
- Zhu, Y., Zhu, X., Zhou, Y., and Zhang, D. (2021). Reduced serum SIRT1 levels in patients with Parkinson's disease: a cross-sectional study in China. *Neurol. Sci.* 42 (5), 1835–1841. doi:10.1007/s10072-020-04711-z